Active magnetic bearings : modelling and control of a five degrees of freedom rotor

de Boer, Wilco

Award date:
1998

7612

Eindhoven University of Technology
Department of Electrical Engineering
Measurement and Control Group

Active Magnetic Bearings: modelling and control of a five degrees of freedom rotor

by ing. W. de Boer

Master of Science Thesis
carried out from March 1998 to December 1998
commissioned by Prof. dr. ir. P.P.J. van den Bosch
under supervision of ir. V.M.G. van Acht
date: December 8, 1998

Summary

For doing research on magnetic bearings, levitation and driving to realise a deflection unit for a 3D laser interferometer, an active magnetic bearing system from the Swiss company MECOS Traxler AG is used. The shaft is borne in five degrees of freedom magnetically and the sixth degree of freedom is driven by an electric motor.

The most simple model for an active magnetic bearing system is a small magnetically conducting ball actively levitated by an electromagnet. Displacements of the ball are measured with a sensor, the sensor signal is the input to a controller. This controller controls the current fed to the electromagnet which closes the loop. When the current is increased, the magnet force increases which makes the ball move towards the coil, this makes the air-gap between the ball and the electromagnet smaller which makes the force even stronger. An active magnetic bearing system is unstable in open-loop.

When this simple model is extended with a second electromagnet the total force acting on the rotor is a function of the displacement in the nominal air-gap and the current. The two poles of the system are symmetric around the imaginary axis and both on the real axis, when examined in the s-domain.

This model can be extended to a fully levitated shaft with six degrees of freedom, five of them magnetically borne. The motions in axial direction can be decoupled from the motions in radial direction. Four degrees of freedom are left for which a model is set-up and a controller is designed. For high rotation speeds the gyroscopic effect (the coupling between the two rotations about the axes perpendicular to the rotation axis of the shaft) stronger. When a complete state space description is set-up the direct transfers consist of four poles and two zeros. Two pole/zero pairs are caused by the non-collocation of the sensor and actuator. Identification of these pole/zero pairs is very difficult. The other two poles are the result of the magnetic levitation.

The identification of an unstable non-linear multiple input multiple output system is hard. Especially when the excitation can be done at one input at a time, only sinusoidal signals can be used and there is not enough memory to store more output signals at a time. However, measuring the closed-loop frequency responses, calculating the open-loop response with the knowledge of the controller and including the knowledge about the steady state gain makes it possible to identify the direct couplings in frequency domain. The indirect couplings can be achieved with the knowledge of the white box modelling.

For an active magnetic bearing system it is useful to use robust controllers, which can handle different loads and rotation speeds. To suppress the gyroscopic couplings the best thing is to use a full multiple input multiple output controller. Since it was not possible to implement in the practical set-up, a multiple input multiple output controller was designed for only the direct couplings and the couplings within the plane. Also this kind of controller seemed to be very promising. When single input single output controllers are designed for multiple input multiple output systems special attention should be paid to the indirect couplings. These can cause the system to become unstable.

Samenvatting

Om onderzoek te kunnen doen naar magnetische lagering, ophanging en aandrijving om zo een reflectie eenheid te kunnen realiseren voor een driedimensionale laser interferometer meter een actief magnetisch gelagerd systeem ontwikkeld door het Zwitserse bedrijf MECOS Traxler AG is gebruikt. De as is in vijf graden van vrijheid magnetisch gelagerd en de zesde graad van vrijheid wordt aangedreven door een moter.

Een heel simpel model voor een actief magnetisch lager is een magnetisch geleidend balletje dat actief wordt opgehangen door de elektromagneet. De verplaatsing van het balletje wordt door middel van een sensor gemeten, dit sensor signaal is de ingang voor een regelaar die op zijn beurt de stroom regelt die door de elektromagneet wordt gestuurd. Op deze manier is de lus gesloten. Wanneer de stroom wordt opgehoogd wordt de kracht sterker. Hierdoor wordt het balletje aangetrokken en wordt de luchtspleet tussen het balletje en de magneet kleiner. Dit kleiner worden van de luchtspleet zorgt ervoor dat de kracht weer groter wordt. Een actief magnetisch gelagerd systeem is in openlus instabiel.

Wanneer dit hele simpele systeem wordt uitgebreid met een tweede elektromagneet dan wordt de totale kracht die werkt op de rotor afhankelijk van de verplaatsing ten opzichte van de nominale luchtspleet en de stroom. De twee polen van het systeem liggen op de reële as en symmetrisch ten opzichte van de imaginaire as, wanneer naar de polen en nulpunten wordt gekeken in het s-vlak.

Het model kan worden uitgebreid naar een volledig gelagerde as met zes graden van vrijheid, vijf van hen worden magnetisch gelagerd. De bewegingen in axiale en radiale richting zijn van elkaar ontkoppeld. Op deze manier blijven vier graden van vrijheid over waarvoor een model moet worden opgesteld en een regelaar moet worden ontwikkeld. Wanneer de as op hoge snelheden rond draait moet ook worden rekening gehouden met gyroscopische effecten, dat wil zeggen indirecte koppelingen binnen het lager. Wanneer de directe overdracht wordt bekeken na het volledig opstellen van een toestandsbeschrijving dan blijken er vier polen en twee nulpunten te bestaan. Twee pool- / nulpunten paren worden veroorzaakt doordat de plaats van de sensor en actuator niet samenvallen. De overige twee polen zijn karakteristiek voor de magnetische ophanging.

De identificatie van een instabiel niet-lineair systeem met meerdere in- en uitgangen is moeilijk. Vooral wanneer slechts één ingang tegelijkertijd kan worden aangestuurd, alleen gebruik kan worden gemaakt van een sinusgenerator en het niet mogelijk is meerdere uitgangen tegelijkertijd op te slaan door geheugen gebrek. Toch is het mogelijk om de identificatie van de directe koppelingen in het frequentie domein te doen door eerst de responsie in gesloten lus te meten, vervolgens de openlus te berekenen door gebruik van de kennis van de regelaar en tenslotte de versterking in rust toe te voegen. De indirecte koppelingen kunnen daarna worden verkregen aan de hand van de kennis van de mathematische beschrijving.

Voor een actief magnetisch gelagerd systeem is het nuttig gebruik te maken van robuuste regelingen om ook de as te kunnen belasten of op hoge snelheden rond te kunnen laten draaien. De gyroscopische koppelingen kunnen het beste worden onderdrukt door gebruik te maken van een volledige regelaar met meerdere in- en uitgangen. Aangezien dit in de praktijk niet mogelijk was is een regelaar ontworpen met twee in- en uitgangen die de directe koppelingen regelt en de koppelingen binnen het vlak van de as. De resultaten hiervan blijken veelbelovend te zijn. Bij het ontwerp van regelaars met maar één ingang en uitgang is het van

"Knowledge of one logically precludes knowledge of the other"

(The Hitch Hikers Guide To The Galaxy, by Douglas Adams, 1979)

Preface

This work has been carried out at the Eindhoven University of Technology, Department of Electrical Engineering, Measurement and Control in a research project on magnetic bearings, levitation and driving to realise a deflection unit for a 3D laser interferometer.

I wish to express my sincere gratitude to Prof. dr. ir. P.P.J. van den Bosch, for giving me the excellent opportunity to carry out this work.

I would like to thank Philips CFT as well, since they made the whole project possible by lending our department the active magnetic bearing. Especially, ir. B. de Veer should be thanked for reviewing this report during the graduation period.

I am also very grateful to my colleagues at the division "Measurement and Control group" for their friendly guidance and assistance. Especially I wish to thank ir. V.M.G. van Acht, he has given me valuable advice concerning my work.

November 23 , 1998, Eindhoven, the Netherlands

Wilco de Boer

Table of contents

LIST OF ABBREVIATIONS IX

LIST WITH EXPLANATION OF WORDS X

1. INTRODUCTION 1

1.1 TASK DESCRIPTION 1
1.2 PRACTICAL SET-UP 2

2. MAGNETIC LEVITATION 3

2.1 SIMPLE MODEL FOR AN ACTIVE MAGNETIC BEARING 3
2.2 FORCES IN THE AMB 3
2.3 EQUATION OF MOTION 5

3. SIX DOF AMB SYSTEM 6

3.1 DECOUPLING OF MOTIONS 6
3.2 EQUATION OF MOTION FOR NON-ROTATING SHAFT 7
3.3 EQUATION OF MOTION FOR THE ROTATING SHAFT 9

4. IDENTIFICATION OF THE ROTOR DYNAMICS 11

4.1 DIFFERENT IDENTIFICATION CONDITIONS 11
4.1.1 Test signals 11
4.1.2 SISO- SIMO, MISO- and MIMO-system identification 11
4.1.3 Open and closed loop identification 12
4.1.4 Identification in the frequency domain or in the time domain 12
4.2 THE USED IDENTIFICATION TECHNIQUE 12
4.3 MEASURED RESPONSES 12
4.3.1 Frequency responses 13
4.3.2 Step responses 13
4.3.3 Results of the measured responses 15
4.4 THE IDENTIFICATION 16
4.5 VALIDATING THE IDENTIFICATION RESULTS 18

5. MIMO-CONTROLLER DEVELOPMENT FOR THE AMB 21

5.1 THE TRACKING PROBLEM 21
5.2 THE AUGMENTED PLANT 23
5.3 CONTROL GOALS AND CONSTRAINTS 25
5.3.1 Stability 25
5.3.2 Tracking 25
5.3.3 Disturbance reduction 25
5.3.4 Sensor noise reduction 26
5.3.5 Actuator saturation avoidance 26
5.3.6 Robustness 26
5.4 SISO-CONTROLLER DESIGN 27
5.4.1 Weighting filters 27
5.4.2 Closed loop performance 28
5.5 MIMO-CONTROLLER DESIGN 31
5.5.1 Weighting filters 32
5.5.2 Closed loop performance 2x2 MIMO controller 33
5.5.3 Closed loop performance 4x4 MIMO controller 34

6. CONCLUSIONS AND RECOMMENDATIONS 36

6.1 OVERVIEW 36
6.2 CHECKLIST 37

BIBLIOGRAPHY 38

APPENDIX A: TAYLOR-EXPANSION **39**

APPENDIX B: MOTIONS AND DISPLACEMENTS **40**

APPENDIX C: INERTIA **41**

APPENDIX D: TRANSFER FUNCTIONS FOR THE IDENTIFICATION **42**

APPENDIX E: SISO CONTROLLER FOR A MIMO SYSTEM **43**

APPENDIX F: RECOMMENDED LITERATURE **45**

List of abbreviations

A/D	Analogue to Digital
AMB	Active Magnetic Bearing
ARX	Auto Regressive Exogenous
ARMAX	Auto Regressive Moving Average Exogenous
D/A	Digital to Analogue
DOF	Degrees Of Freedom
DSP	Digital Signal Processor
EPROM	Electrical Programmable Read Only Memory
FDC	Fast Digital Controller
FRF	Frequency Response Function
I/O	Input / Output
MIMO	Multiple In Multiple Out
MISO	Multiple In Single Out
OE	Output Error
PC	Personal Computer
PRBN	Pseudo Random Binary Noise
RAM	Random Access Memory
RPM	Rotation Per Minute
SIMO	Single In Multiple Out
SISO	Single In Single Out

List with explanation of words

Gyroscopic effect	This can be best explained by using a small example [ROE90]. When you for example sit on a desk-chair (an expensive one that can rotate), you hold between your hands a big fast rotating wheel (e.g. bicycle wheel) and you will do the following experiment. Turn the wheel in a clock-wise direction then you will notice that your chair is turning also. The direction of this depends on the direction in which your wheel was rotating. So the coupling between two of these planes is called the gyroscopic effect.
Thrust bearing	This bearing prevents axial movements.
Weighting filters	Filters that characterise the in- or output signals, normally used in robust control design.
White noise	Time signals are white noise signals when the frequency spectrum has the same power amplitude over a large (equal or greater than the bandwidth) frequency band.

1. Introduction

The Measurement and Control Group of the Eindhoven University of Technology is doing research on magnetic bearings, levitation and driving to realise a deflection unit for a 3D laser interferometer. This will be a free floating mirror that will be actively magnetically borne in three degrees of freedom (DOF), in two DOF active magnetically driven and in the last DOF passive magnetically damped. The position inaccuracy of the mirror has to be smaller then 1 μm and the orientation inaccuracy has to be smaller then 1 μrad. The angular range of the mirror should be 1 rad for the two actively controlled rotations. Finally the bandwidth of the controlled system should be more than 100 Hz.

As a first pilot project for this active magnetically borne and driven mirror a magnetic levitation system has been developed, with one DOF. (An iron ball under an I-shaped coil). With the purpose to minimise the dimensions of the mirror, the self-sensing levitation principle is examined. It is shown that with this self-sensing principle the desired accuracy can not be reached.

As a second pilot project, for this magnetically borne mirror, a magnetically borne shaft from the Swiss company MECOS Traxler AG is borrowed from Philips CFT. This shaft is specially developed as a study model. The shaft is in five DOF magnetically borne and is driven by an asynchronous motor with a maximum rotation speed of 30.000 rpm. The supporting sensors, actuators, electronics and signal-processors are also delivered by MECOS Traxler AG. This practical set-up was obtained from MECOS Traxler AG and is described in detail in section 1.2, but first the graduation project will be explained in more detail.

1.1 Task description

The graduation project consists of several parts.

1. Set-up a mathematical model for the motions of the shaft, take into account that the shaft is rotating;
2. A mathematical derivation of the MIMO-transfer-function (Multiple In Multiple Out) of the actuator currents to the sensor displacements, take into account that the non-linear relationship between force and current/position of the actuators;
3. Black-box identification of the shaft, take into account that the fact that the bearing system is open-loop unstable;
4. Implementing the mathematical model of the shaft in Simulink and comparing this with the model obtained by the black-box identification;
5. Designing a MIMO-controller for the shaft and simulating the controller in Simulink;
6. (If hardware permits ...) Implement the designed controller in the digital signal-processor;
7. It is appreciated if a short and clear manual for the MECOS Traxler AG-software (Matlab toolbox) is written.

The first two parts are described in the chapters 2, in which a simple model explains the magnetic levitation principle, and 3, in which the complete equation of motion for five degrees of freedom (DOF) is derived. The identification process is described in chapter 4. Finally in chapter 5 the developed controller is described.

The last part is not described in this report but a separate report [BOE98] is written for this.

1.2 Practical set-up

The Active Magnetic Bearing (AMB) system obtained from MECOS Traxler AG is the "miniVS: configuration C3". This system consists of a hardware part and a software toolbox for Matlab™[1].

The hardware of the miniVS, configuration 3 consists of the following: the control cabinet (MBE8/50), a frequency converter (CF200) and the magnetically borne shaft. In the block diagram below the complete system is shown.

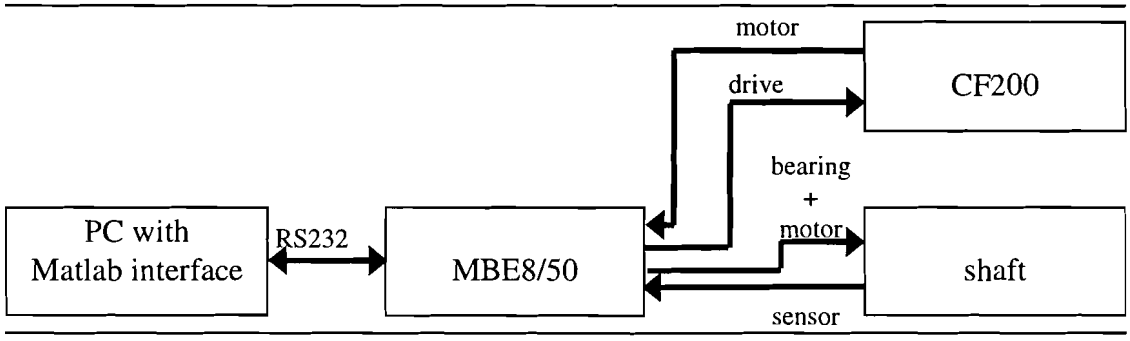

Figure 1-1, block diagram

The control cabinet consists of:

- sensor electronics for 5 displacement sensors and the rotational pulse;
- a fast digital controller (FDC) board based on the TMS320C25 signal processor with 8 input channels (A/D), 12 output channels (D/A), digital I/Os and serial/parallel interface to the personal computer;
- 10 pulse width modulated power amplifier channels with a maximum output power of 300 [W] each (50 [V], 6 [A]).

The displacement sensors all utilise the measurement principle of Eddy current. They have a resolution of 200 [nm] and a linearity error smaller then 10%.

The A/D converters (including multiplexer) and the D/A converters, on the FDC board, have a resolution of 12 bits. The program and control parameters are stored in an EPROM. The memory on the FDC board is divided in a 32kWord EPROM (one word is equal to 16 bits), a 32kWord RAM (for the program) and a 64kWord RAM (for the data).

The pulse width modulated power amplifiers have a modulation frequency of 78.125 kHz, a maximum output current of 6A and are current controlled.

The interface between Matlab™ and the controller board (MBE8/50), the variables of the AMB controller board can be accessed by name through a hidden cross reference table. This cross reference table not only manages the bookkeeping of memory addresses and variable names, but also enables the use of vector and matrix objects of variable size for controller downloading.

The Matlab™ interface also incorporates tools for taking real time history measurements of AMB controller variables. For this purpose, the digital controller can be configured to store up to 50000 samples in the on-board memory.

---

[1] Matlab is a trademark of The MathWorks inc.

2. Magnetic levitation

Since an active magnetically borne shaft is quite complicated, this chapter will introduce a very simple model of an Active Magnetic Bearing (AMB) system. This model will be used for a first set-up of the mathematical description of an AMB system with six degrees of freedom (DOF). Section 2.1 will give a description of the simple model and explain all the important components in an AMB system. The following section will explain of which physical parameters the forces acting on the shaft are dependent. Finally, in section 2.3, a first equation of motion is introduced.

2.1 Simple model for an Active Magnetic Bearing

The most simple model for an AMB system (see Figure 2-1) is a rotor that is actively levitated by one magnetic force. The working of this AMB system is described below.

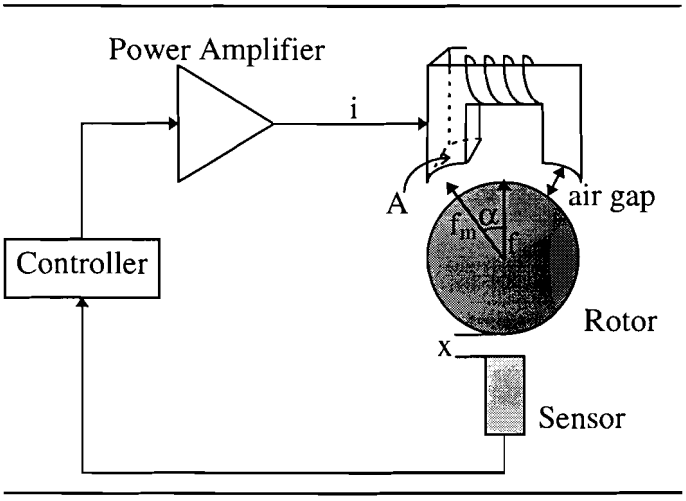

Figure 2-1, simple model of AMB

The sensor measures the displacement x of the supported rotor. A controller, for example a microprocessor, uses this information to derive an appropriate signal which is fed to a power amplifier. The amplified signal drives the control current in the coil, causing a magnetic force to act on the rotor. The electromagnetic force has to be calculated by the controller in such a way, that the rotor remains in its predefined and stable hovering position.

2.2 Forces in the AMB

A simple topology for an active magnetic bearing is already described in the previous section. Figure 2-1 shows an electromagnet which is supplied with a current i. The current flowing through the coil will give rise to the flux Φ, which generates attracting forces. The law of Hopkinson [VAN96] is given by:

$$\Phi_c \sum R_m = Ni,$$

here is N the number of windings, i the current through the coil, Φ_c the circuit-flux and R_m the magnetic resistance. R_m is approximately given by:

$$R_m = \frac{x_0 + \Delta x}{\mu_0 A},$$

here x_0 is the nominal air-gap, Δx the displacement from the nominal air-gap, μ_0 the permeability of air and A the area of the magnet through which the flux flows. This formula is only valid when the magnetic resistance of the iron circuit is neglected.

The total magnetic flux Φ is given by: $\Phi = N\Phi_c$, the main inductivity is given by:

$$L_m = \Phi/i = \frac{N^2 i \mu_0 A}{2(x_0 + \Delta x) i} = \frac{N^2 \mu_0 A}{2(x_0 + \Delta x)} \text{ . [H]}$$

In the function for the main inductivity i is cancelled out because linear magnetic material is assumed. The magnetic force f_m is calculated by the deviation to x of the field energy:

$$f_m = -\tfrac{1}{2} i^2 \frac{\partial L_m}{\partial x} \text{ . [N]}$$

The angle between f and f_m, in Figure 2-1 will be called α. Then the vertical force f is:

$$f = \cos\alpha \; f_m = \cos\alpha \frac{N^2 \mu_0 A}{4} \left(\frac{i}{x_0 + \Delta x} \right)^2 \text{ . [N]}$$

The term before the brackets will be called K.

Figure 2-1 can be extended into Figure 2-2. This shows two electromagnets both with the same initial current. The extension is necessary since an electromagnet can only pull and the movement of the shaft should be in both directions. This initial current is applied to give a certain premagnetization, which is applied to put the working point on a linear trajectory.

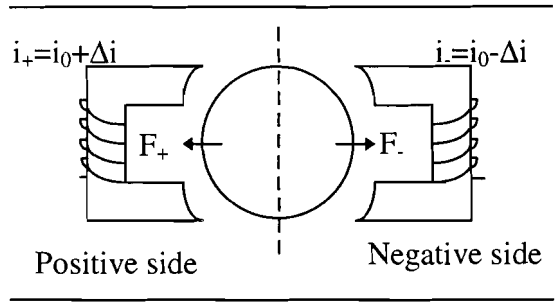

Figure 2-2, extension with a second electromagnet

The two functions for the forces will be given by:

$$F_+ = K\left(\frac{i_0 + \Delta i}{x_0 - \Delta x} \right)^2 \text{ and } F_- = K\left(\frac{i_0 - \Delta i}{x_0 + \Delta x} \right)^2 .$$

Pay attention to the plus- and minus-signs in the equations. The total force F_t will be the difference between F_+ and F_-, the resulting function can be approximated by a first order Taylor-expansion, under the assumptions that $\Delta x << x_0$ and $\Delta i << i_0$.

The linear function that follows is:

$$F_t \approx \frac{4Ki_0^2}{x_0^3}\Delta x + \frac{4Ki_0}{x_0^2}\Delta i = K_x \Delta x + K_i \Delta i \text{ . } \quad (2\text{-}1)$$

For the derivation is referred to Appendix A.

The total force acting on the rotor is thus a function of the displacement in the nominal air-gap and the current. The K_s term is positive which means that the system has a negative stiffness and thus is unstable. The K_i term is the proportional actuator gain for the current request of the controller. The above relations do not take into account the resistance of the coil, stray field effects, iron saturation effects, hysteresis effects and Eddy current losses.

2.3 Equation of motion

For controlling the system, brought up in the introduction of this chapter, the output variable will be the displacement Δx and the input variable the current Δi. The second law of Newton is:

$$\vec{F} = m\vec{a}\,.$$

In our model the acceleration $\vec{a}$ is given by $\ddot{x}$, $\vec{F}$ is the force given by equation (2-1) and m is the mass. Substituting (2-1) in Newton's equation gives

$$m\Delta\ddot{x} - K_s\,\Delta x = K_i\Delta i\,.$$

At this point it can be made clear that control for an AMB system is necessary. Without any control ($K_i\,\Delta i = 0$) the slightest deviation from the equilibrium x_0 will result in an instantaneous exponential increase of $\Delta x(t)$, because $K_s > 0$. Either the rotor hits the magnet or it falls down. In the example above the gravity is neglected.

The differential equation, brought up above, can be transposed to the state space description:

$$\dot{\mathbf{x}} = \mathbf{Ax} + \mathbf{Bu}$$
$$\mathbf{y} = \mathbf{Cx} + \mathbf{Du}$$

where the state space vector is given by:

$$\mathbf{x} = (\Delta x \quad \Delta\dot{x})^T\,,$$

the input vector $\boldsymbol{u}$ is the current Δi and the output vector $\boldsymbol{y}$ is the displacement Δx. The matrices will then become:

$$A = \begin{pmatrix} 0 & 1 \\ \dfrac{K_s}{m} & 0 \end{pmatrix} \qquad B = \begin{pmatrix} 0 \\ \dfrac{K_i}{m} \end{pmatrix} \qquad C = \begin{pmatrix} 1 & 0 \end{pmatrix} \qquad D = (0).$$

The state space description above can be used to design a controller for the AMB system. The eigenvalues of the A matrix are the poles of the system. The poles are $+\sqrt{\dfrac{K_s}{m}}$ or $-\sqrt{\dfrac{K_s}{m}}$, the one in the right half plane (s-domain), see Figure 2-3, indicates that the system is unstable.

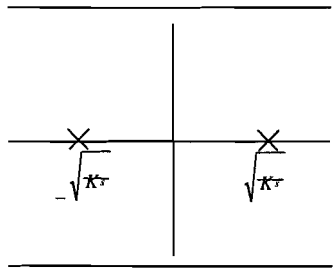

Figure 2-3, pole/zero map

3. Six DOF AMB system

In this chapter the complete shaft with six degrees of freedom (DOF) is introduced. This shaft can freely translate and also rotate in three directions. To explain these motions first a co-ordinate system will be defined, see Figure 3-1. This shaft is levitated by an AMB system. For this, the simple model of the previous chapter should be extended with more magnetic bearings.

Only five of these motions can be controlled, the sixth is the rotation around the z-axis and this one is controlled by the motor. The other five, rotations around the x- and y-axis and the translations along the x-, y- and z-axis, should be controlled by the AMB system.

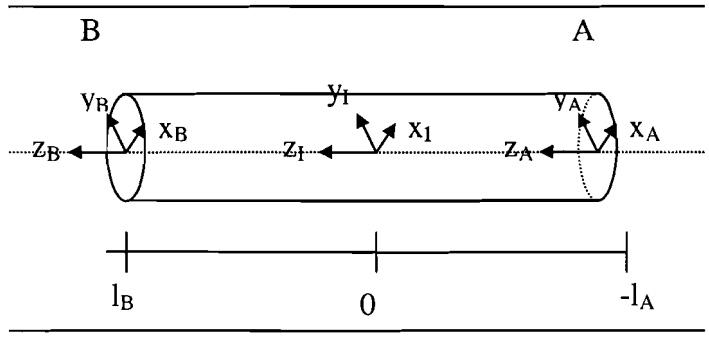

Figure 3-1, the rotor with its co-ordinate system

When all effects are included, the rotordynamics are quite complex equations. For this, the chapter is split up in several sections. In section 3.1 the possibility of decoupling some of the motions is described. In the following two sections (3.2 and 3.3) the equations of motion are derived for non-rotating and rotating shafts.

3.1 Decoupling of motions

Before the equations of motion can be given, it has to be checked which rotations or translations affect the others. Assumed is that deviations from the reference position are small compared to the rotor dimensions. This allows a linearization of the equations of motion [SCH94]. The arrangement of the bearings is such that the force vector of the thrust bearing (axial bearing) acts along a line through the centre of mass. Under this assumption, the motions in axial direction are independent of motions in the radial direction. This subsystem may therefore be separated from the remaining four degrees of freedom. For low speed rotations there is no gyroscopic effect and the rotations about the x-axis and y-axis can also be assumed to be decoupled. The small motions of the rotor are described by the displacements x_S, y_S, z_S of its centre of mass S with respect to the inertial reference $O\text{-}x_I y_I z_I$ and by its inclinations α,β,γ about the x_I-, y_I- and z_I- axis. The angular velocity of the rotor about its longitudinal axis is $\dot{\gamma} = \Omega$ (see Figure 3-2).

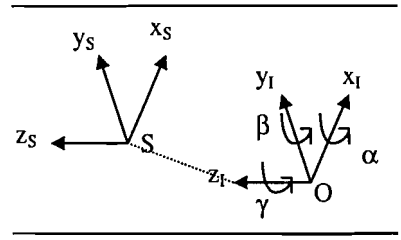

Figure 3-2, small motions

3.2 Equation of motion for non-rotating shaft

From the six DOF we need to examine only four at a time, two translations along and two rotations about the x- and y-axis. For these motions one equation should be set-up.

The equation of motion is:

$$\mathbf{M}\ddot{\mathbf{q}} = \mathbf{F}\,.$$

This matrix equation will be explained in the following paragraphs.

The four DOF are described in the vector

$$\mathbf{q} = \begin{bmatrix} \beta & \Delta x & -\alpha & \Delta y \end{bmatrix}^T,$$

where for the minus-sign, before the angle α, is referred to Appendix B. The mass and inertia matrix

$$\mathbf{M} = \begin{pmatrix} J_y & 0 & 0 & 0 \\ 0 & m & 0 & 0 \\ 0 & 0 & J_x & 0 \\ 0 & 0 & 0 & m \end{pmatrix} = diag[J_y, m, J_x, m]\,,$$

is symmetric and positive definit ($\mathbf{M} = \mathbf{M}^T > 0$), because $\boldsymbol{M}$ is diagonal and each of the elements is greater than zero. The inertia J_y is equal to the inertia J_x because the rotor is assumed to be symmetric.

Finally, the generalised force/torque $\boldsymbol{F}$ (for small α and β),

$$\begin{pmatrix} F_1 \\ F_2 \\ F_3 \\ F_4 \end{pmatrix} = \mathbf{F} = \tilde{\mathbf{B}}\mathbf{u}_f\,, \qquad \tilde{\mathbf{B}} = \begin{pmatrix} l_B & l_A & 0 & 0 \\ 1 & 1 & 0 & 0 \\ 0 & 0 & l_B & l_A \\ 0 & 0 & 1 & 1 \end{pmatrix}.$$

In this equation the radial bearing forces are represented in a general way by four control forces, which act within the bearing planes in the x_I- and y_I-directions,

$$\mathbf{u}_f = \begin{bmatrix} f_{x,B} & f_{x,A} & f_{y,B} & f_{y,A} \end{bmatrix}^T.$$

Two types of equations can be recognised in the equation of motion. The first one is given by

$$m\Delta\ddot{x} = f_{x,B} + f_{x,A}$$

and the second one is given by

$$J_y\ddot{\beta} = l_B f_{x,B} + l_A f_{x,A}\,.$$

The first one can be recognised as Newton's second law of motion while the second one can be recognised as the Euler's second law of motion. The lengths l_A and l_B are the distances between the centre of mass and the bearings.

Each bearing force is composed of a current dependent term and a displacement dependent term. In the linearised form this is a simple sum, as introduced in equation (2-1):

$$\mathbf{u}_f = \mathbf{K}_s \mathbf{q}_{rotor} + \mathbf{K}_i \mathbf{i}$$

The vector $\boldsymbol{q}_{rotor}$ expresses the rotordisplacements in terms of the bearing displacement.

$$\mathbf{q}_{rotor} = \begin{bmatrix} x_B & x_A & y_B & y_A \end{bmatrix}^T = \begin{pmatrix} l_b & 1 & 0 & 0 \\ l_a & 1 & 0 & 0 \\ 0 & 0 & l_b & 1 \\ 0 & 0 & l_a & 1 \end{pmatrix} \mathbf{q} = \mathbf{T}_{rotor}\mathbf{q}.$$

The force displacement coefficients and force current coefficients of each bearing are grouped in the diagonal matrices $\boldsymbol{K}_S$ and $\boldsymbol{K}_i$.

$$\mathbf{K}_S = \begin{pmatrix} k_{s,a} & 0 & 0 & 0 \\ 0 & k_{s,b} & 0 & 0 \\ 0 & 0 & k_{s,a} & 0 \\ 0 & 0 & 0 & k_{s,b} \end{pmatrix}, \quad \mathbf{K}_i = \begin{pmatrix} k_{i,a} & 0 & 0 & 0 \\ 0 & k_{i,b} & 0 & 0 \\ 0 & 0 & k_{i,a} & 0 \\ 0 & 0 & 0 & k_{i,b} \end{pmatrix}.$$

The complete equation of motion will become:

$$\ddot{\mathbf{q}} = \mathbf{M}^{-1}\,\tilde{\mathbf{B}}\,\mathbf{K}_s\mathbf{T}_{rotor}\mathbf{q} + \mathbf{M}^{-1}\tilde{\mathbf{B}}\,\mathbf{K}_i\mathbf{i}$$

Now a state vector $\boldsymbol{x}$ will be introduced of bearing displacements and their derivatives, so a state-space description can be set-up. The state vector will then become:

$$\mathbf{x} = \begin{bmatrix} \beta & \Delta x & -\alpha & \Delta y & \dot{\beta} & \Delta\dot{x} & -\dot{\alpha} & \Delta\dot{y} \end{bmatrix}^T,$$

the input vector:

$$\mathbf{u} = \begin{bmatrix} i_{x,B} & i_{x,A} & i_{y,B} & i_{y,A} \end{bmatrix}^T$$

and the output vector will be the rotor displacements at the sensors:

$$\mathbf{y} = \begin{bmatrix} \Delta x_D & \Delta x_C & \Delta y_D & \Delta y_C \end{bmatrix}^T.$$

The state-space description will finally become:

$$\begin{aligned} \dot{\mathbf{x}} &= \mathbf{A}\mathbf{x} + \mathbf{B}\mathbf{u} \\ \mathbf{y} &= \mathbf{C}\mathbf{x} + \mathbf{D}\mathbf{u} \end{aligned}.$$

The matrices in the state-space description will be:

$$\mathbf{A} = \begin{pmatrix} \mathbf{0} & \mathbf{I} \\ \mathbf{M}^{-1}\tilde{\mathbf{B}}\mathbf{K}_s\mathbf{T}_{rotor} & \mathbf{0} \end{pmatrix} \quad \mathbf{B} = \begin{pmatrix} \mathbf{0} \\ \mathbf{M}^{-1}\tilde{\mathbf{B}}\mathbf{K}_i \end{pmatrix} \quad \mathbf{C} = \begin{pmatrix} l_D & 1 & 0 & 0 & \\ l_C & 1 & 0 & 0 & \mathbf{0} \\ 0 & 0 & l_D & 1 & \\ 0 & 0 & l_C & 1 & \end{pmatrix} \quad \mathbf{D} = (\mathbf{0}).$$

In the matrix $\boldsymbol{C}$ the lengths l_C and l_D are the distances between the centre of mass and the sensors. When the variables are filled in, according to Appendix C, the eigenvalues of A are:

$$\begin{bmatrix} 582.3652 \\ -582.3652 \\ 582.3652 \\ -582.3652 \\ 372.7214 \\ -372.7214 \\ 372.7214 \\ -372.7214 \end{bmatrix}.$$

The pole/zero map is given in Figure 3-3.

3.3 Equation of motion for the rotating shaft

To extend the equation of motion from the previous section to an equation which includes the gyroscopic effect the same steps should be taken, but now started with the equation

$$\mathbf{M}\ddot{\mathbf{q}} + \mathbf{G}\dot{\mathbf{q}} = \mathbf{F}.$$

The gyroscopic matrix,

$$\mathbf{G} = \begin{pmatrix} 0 & 0 & 1 & 0 \\ 0 & 0 & 0 & 0 \\ -1 & 0 & 0 & 0 \\ 0 & 0 & 0 & 0 \end{pmatrix} J_z \Omega,$$

is skew-symmetric ($\mathbf{G} = -\mathbf{G}^T$) and contains the rotor speed Ω as a linear factor. The gyroscopic effect is given by

$$f_{x,B} l_B + f_{x,A} l_A = -\dot{\alpha} J_z \Omega,$$

which couples the *xz*- and *yz*-plane.

The complete equation of motion yields:

$$\ddot{\mathbf{q}} = -\mathbf{M}^{-1}\mathbf{G}\dot{\mathbf{q}} + \mathbf{M}^{-1}\tilde{\mathbf{B}}\mathbf{K}_s\mathbf{q} + \mathbf{M}^{-1}\tilde{\mathbf{B}}\mathbf{K}_i\mathbf{i},$$

with the gyroscopic effect included.

The matrices in the state-space description are:

$$\mathbf{A} = \begin{pmatrix} \mathbf{0} & \mathbf{I} \\ \mathbf{M}^{-1}\tilde{\mathbf{B}}\mathbf{K}_s\mathbf{T}_{rotor} & -\mathbf{M}^{-1}\mathbf{G} \end{pmatrix} \quad \mathbf{B} = \begin{pmatrix} \mathbf{0} \\ \mathbf{M}^{-1}\tilde{\mathbf{B}}\mathbf{K}_i \end{pmatrix} \quad \mathbf{C} = \begin{pmatrix} l_D & 1 & 0 & 0 & \\ l_C & 1 & 0 & 0 & \\ 0 & 0 & l_D & 1 & \mathbf{0} \\ 0 & 0 & l_C & 1 & \end{pmatrix} \quad \mathbf{D} = (\mathbf{0}).$$

The pole-zero map for the direct coupling is given in Figure 3-3. The two most inner pole and

zero pairs are caused by the non-collocation of the sensor and the magnetic bearing

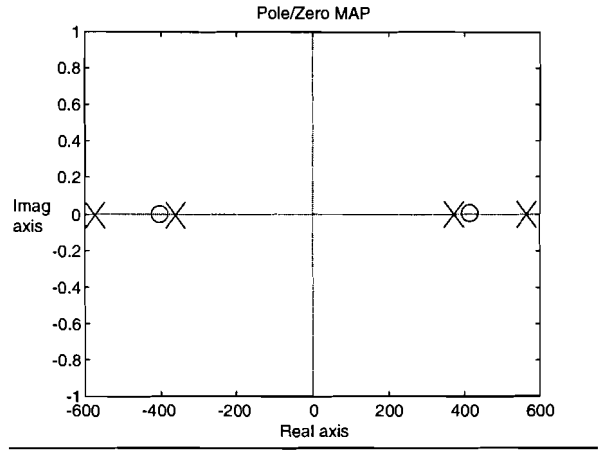

Figure 3-3, typical pole/zero map

($l_a \neq l_c \wedge l_b \neq l_d$). The most outer poles are the result of the magnetic levitation principle introduced in the previous chapter. These poles will become slightly complex (Im << Re) when the speed is increased.

Since the axis is assumed to be symmetric and the centre of mass is almost in the middle of the shaft all four direct transfers are almost the same. In Figure 3-4 the frequency response is given for the four different couplings.

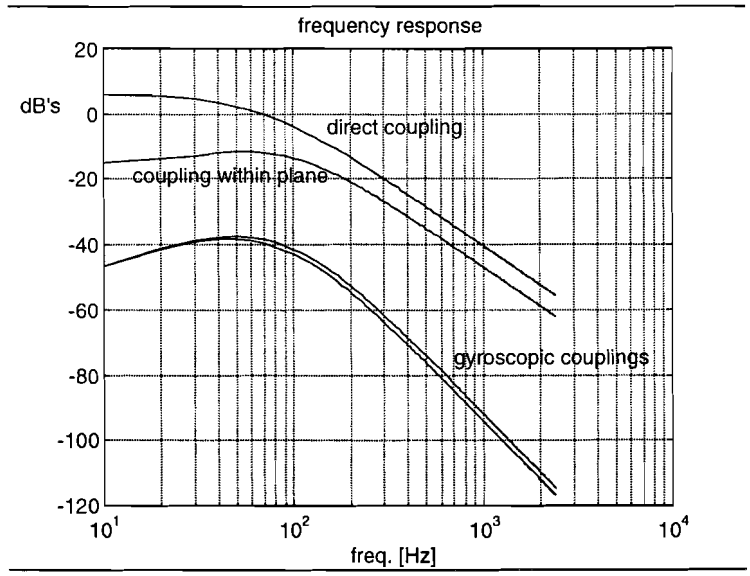

Figure 3-4, frequency responses

The couplings are defined as follows:

Direct coupling	$x_a \rightarrow x_a$	$x_b \rightarrow x_b$	$y_a \rightarrow y_a$	$y_b \rightarrow y_b$
Coupling within plane	$x_a \rightarrow x_b$	$x_b \rightarrow x_a$	$y_a \rightarrow y_b$	$y_b \rightarrow y_a$
Coupling within bearing (gyroscopic)	$x_a \rightarrow y_a$	$x_b \rightarrow y_b$	$y_a \rightarrow x_a$	$y_b \rightarrow x_b$
Coupling within other bearing (gyroscopic)	$x_a \rightarrow y_b$	$x_b \rightarrow y_a$	$y_a \rightarrow x_b$	$y_b \rightarrow x_a$

4. Identification of the rotor dynamics

To design a controller an accurate model of the shaft is needed. In the previous chapter a mathematical model was derived for the motions of the rigid shaft. In this chapter the identification of the practical system is described. The model of the previous chapter will further on be referred to as the white box model and the model that is derived in this chapter the black box model, for the time being. The physical parameters for the white box model are available using the technical specifications of the practical set-up.

Since many identification algorithms and techniques have been developed in the last decades, a proper one should be chosen. The considerations are done in section 4.1.

4.1 Different identification conditions

Identification of the black box model can be done in the frequency domain or in the time domain. Various identification algorithms are available for this. For example in the time domain there are model sets available like ARX, ARMAX and OE. Besides the various algorithms there are also many possibilities for the test signals, are PRBN-signals, sinusoidal signals or multi-sinusoidal signals used? Is the identification done for a SISO-, SIMO, MISO or MIMO-system. Also an important question is whether the identification should be done closed loop or open loop. All these conditions together give many identification methods. In the following subsection many of these possible choices are described with their advantages and disadvantages.

4.1.1 Test signals

PRBN test signals are block signals with a varying period time, the variation of this period time makes the signal have a white noise frequency spectrum. PRBN test signals should be white noise for at least the bandwidth of the open loop system. For making block-signals each sample (a transition from 1→0 or 0→1) should be written from the PC over the serial link to the DSP. This communication is too slow to make high frequency block signals (> 200 [Hz]).

Sinusoidal test-signals can be used since the DSP, used for controlling the AMB, has a sine-wave generator implemented in software. However, multi-sinusoidal test signals are not possible because the sine-wave generator can only generate one signal with a specific frequency at a time and so multi-sinusoidal test-signals have to be generated by the PC. This will introduce the same problem as the PRBN test signals gave.

The only possible test signals with high frequencies that can be used are sinusoidal signals. The lowest frequency possible for using the sinusoidal signals is dependent of the amount of memory available to store samples and sample time.

4.1.2 SISO- SIMO, MISO- and MIMO-system identification

The AMB-system has it shortcomings for identification, independent excitations of more than one input is not directly possible. This makes MISO and MIMO identification inconvenient and only SIMO or SISO identification remains. Since there is a limited amount of memory to store sampled data and it is important to identify accurately at low frequencies the SISO identification is preferred.

Excitation of more than one input at a time is possible when the controllers are extended with some oscillating filters. This makes the order of the implemented controllers higher. To

change the frequency the filters should be changed each time, this is a very time consuming way for the identification.

4.1.3 Open and closed loop identification

The open loop process that should be modelled is unstable and because of this it must be identified in closed loop, so there cannot be done a direct excitation on the input of the process. Because of this, the inputs and outputs of the closed loop should be measured. Since the controller used in the closed loop is exactly known (downloadable from the DSP) the open loop model can be calculated from the closed loop identification.

The above described method is called the indirect method, the direct method is also tried but gave less accurate results than the indirect method.

4.1.4 Identification in the frequency domain or in the time domain

As already said the identification can be done in the two domains, the time domain and the frequency domain. In the previous sub-section it has been made clear that the excitations and measurements should be done in closed loop. When the time domain identification is used the model that is derived consists of poles and zeros in either the z- or s-plane. When the open loop is calculated with the knowledge of the controller, the poles and zeros of the controller will not cancel out the poles and zeros of the open-loop model because the identified model does not exactly describe the process.

In the frequency domain this problem can be avoided by measuring for each frequency the closed loop transfer. In this case the open-loop can be calculated in the frequency domain point by point and then an identification algorithm can be started.

It should be mentioned that the frequency response identification technique is most widely used for AMB systems. This technique can be used for SISO systems [GAH95] as well as for MIMO systems [GAH97].

4.2 The used identification technique

Summarising the results of the previous sections makes clear that SISO identification should be used based on the frequency responses with sinusoidal test signals. The actual identification is done with the open loop frequency response function which is obtained by measuring the closed loop. SISO identification means that there should be measured sixteen responses of the closed loop system.

4.3 Measured responses

To validate later on the identified process different responses are measured in forehand. A validation can be done by examining the step responses of the closed loop system. The fit in the frequency domain is already good because the algorithm used is trying to fit the model to the measurements. The steady state gains can be determined quite well examining the difference between the input of the plant (current) and the output (displacement) when a step response is done. This is necessary because low frequency measurements are disturbed and not measurable because of memory restrictions. Also the frequency response is a valuable response for validating the identified model. Both of these responses are described in the following two sub-sections, while in the last sub-section the results are given. In Figure 4-1 the block diagram of the SISO closed loop system is given to which is referred in the next sub-sections. Pay attention that the plus and minus signs are switched compared to the general

structure normally used.

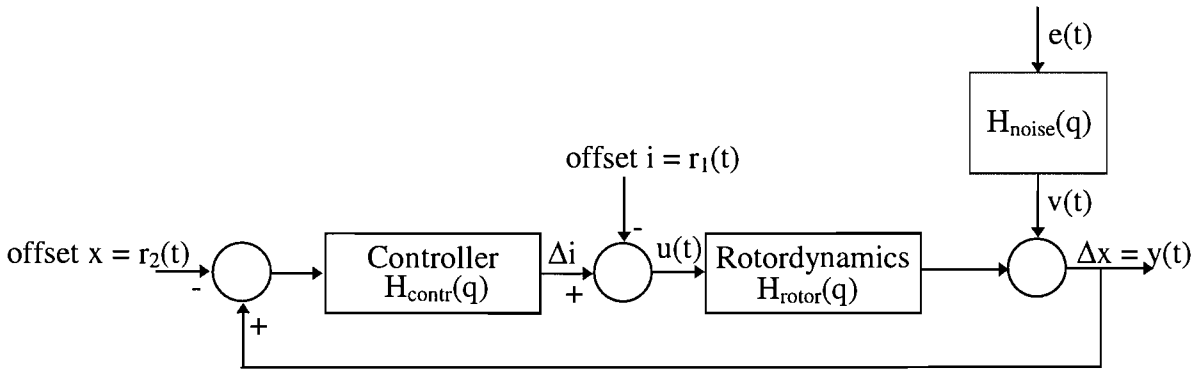

Figure 4-1, block diagram of the SISO transfer

4.3.1 Frequency responses

The frequency response is measured by a sinusoidal excitation on the input and measuring the response at the output for different frequencies. For each of these frequencies the gain and phase between the input and output is calculated. This response is plotted in bode-diagrams (see Figure 4-2, Figure 4-3, Figure 4-4 and Figure 4-5). There is not much difference between the excitation on the different inputs and their responses on the outputs, so only four responses are given (one direct coupling , one coupling within the plane, one coupling within the bearing and finally the coupling in the bearing on the other side). The reference $r_1(t)$ will be used for

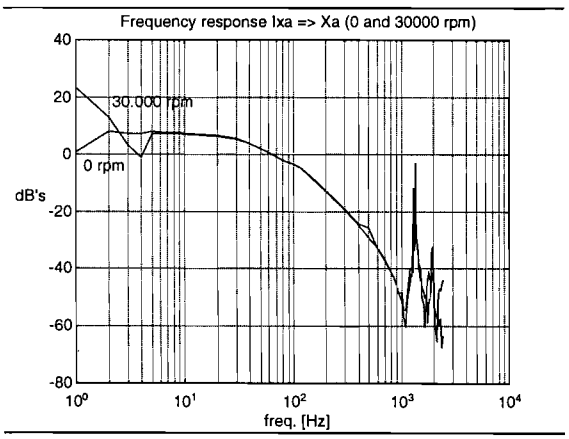

Figure 4-2, direct coupling

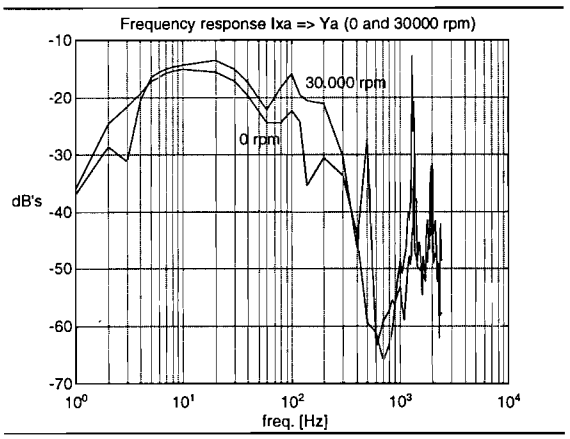

Figure 4-3, coupling within bearing

the input and the displacements $y(t)$ are measured.

The gyroscopic couplings $\left(\Delta y_a / i_{X,a} \text{ and } \Delta y_b / i_{X,a} \right)$ become more important when the rotation speed gets higher.

4.3.2 Step responses

As already mentioned in the previous sub-section, there is not much difference between the excitation on the different inputs and their responses on the outputs, so only four

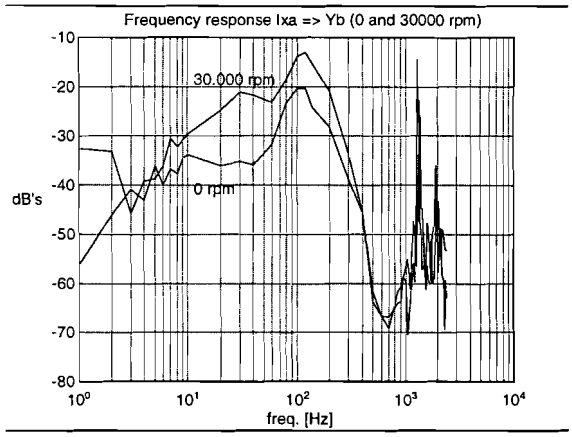

Figure 4-4, coupling within other bearing

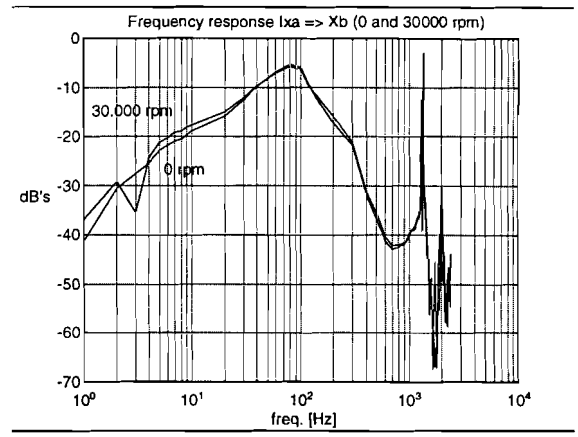

Figure 4-5, coupling within plane

displacements are measured (the direct coupling, the coupling within the plane, the coupling within the bearing and finally the coupling in the bearing on the other side). The reference $r_2(t)$ will be used for the input and the displacements are measured. The step will be about 24 µm high (equal to 24.4 [µm] divided by 122 [nm] equals 200 DSP units). The step response

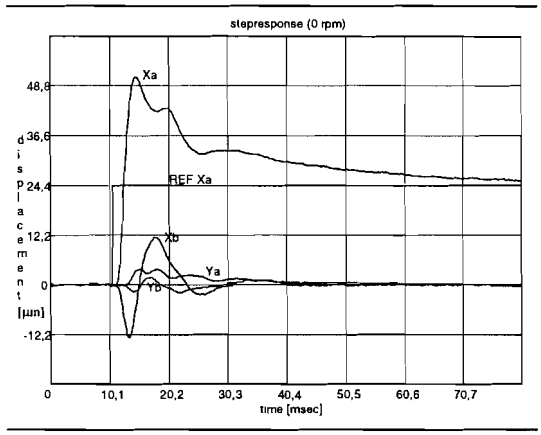

Figure 4-6, step response (0 rpm)

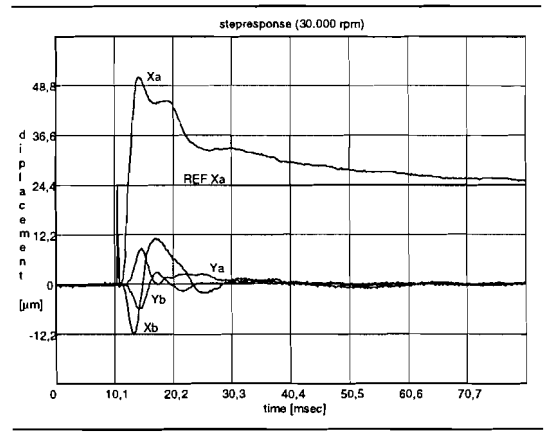

Figure 4-7, step response (30.000 rpm)

measured at 0 rpm and 30.000 rpm are plotted in Figure 4-6 and Figure 4-7. Again the gyroscopic coupling becomes bigger when the shaft is rotating at a higher speed.

This step response is a useful validation tool for the identified model later on.

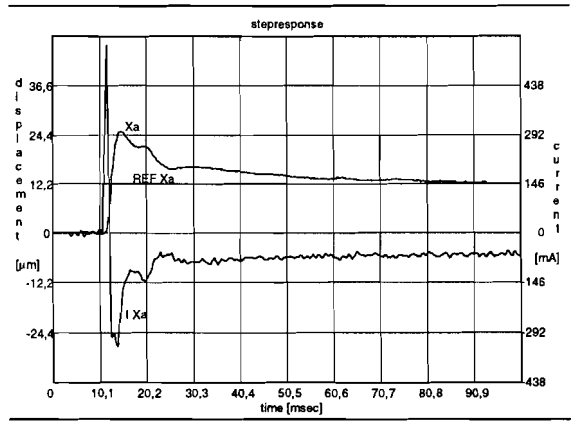

Figure 4-8, step response to determine gain

To determine the steady state gain the step response is used. Again the reference signal $r_2(t)$ is changed, now only from zero to 12,2 [μm]. When the relationship between the current and the reference is examined the steady state gain can be determined (see Figure 4-8).

4.3.3 Results of the measured responses

The main thing that catches the eye is the coupling between the *X*- and *Y*-plane while the shaft was not rotating. The coupling is as big as the coupling caused by the gyroscopic effect (at maximum rotational speed). This extra coupling, which was not taken into account in the theoretical model, occurs by three phenomena. First there is the thrust bearing which gives an extra coupling, secondly the motor gives an extra coupling. The existence of these two phenomena can be shown by turning off the motor and the thrust bearing. The influences of these two phenomena are shown in Figure 4-9.

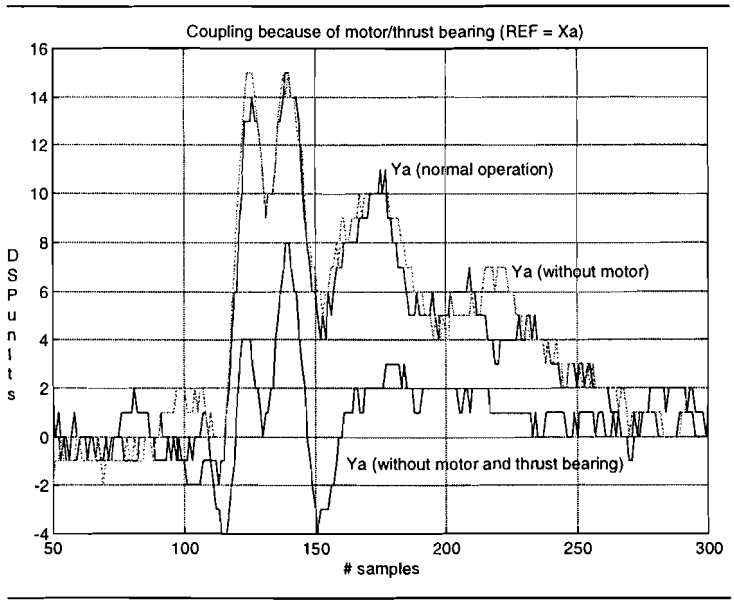

Figure 4-9, influence of thrust bearing and motor

The occurrence of the small coupling finally left can be explained Figure 4-10.

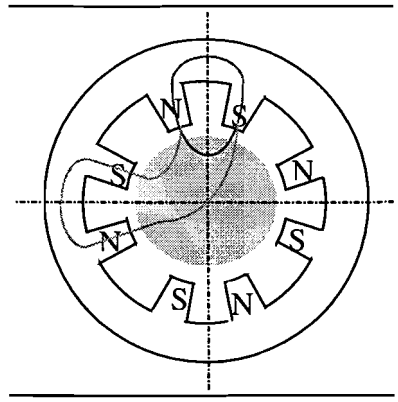

Figure 4-10, magnetic bearing

In Figure 4-10 two flux lines are shown, one coloured dark grey and one light grey. The dark one is the normal flux line, following the shortest path, caused by the electrical current flowing through the coils. The light grey is an example of leakage. Many of these magnetic flux lines can be drawn in Figure 4-10. All of these leaking flux lines are symmetric since the

whole magnetic bearing is symmetric. When the shaft is not exactly in the middle (or not exactly symmetric) the leaking flux lines will also be part of the attraction of the shaft, because the flux is not symmetric. This phenomena is making the coupling between the *X*- and *Y*-plane. This has been checked by measuring the influence of a step response (e.g. *X*-axis) on the coupling within the bearing (e.g. *Y*-axis) and comparing this with the influence of a step response (e.g. *X*-axis) on the coupling within the bearing (e.g. *Y*-axis) when the shaft is deliberately displaced in e.g. the *Y*-axis.

Further on, it should be noted that the two pole/zero-pairs (see Figure 3-3) can not be identified from the frequency response (no bumps are visible). Both of these pairs are the result of non-collocation of the sensor and active magnetic bearing. Since these pole/zero pairs can not be identified from the frequency response it is also a problem to control them, although they are not controlled the system will not become unstable. This will be explained using Figure 4-11, which shows the whole shaft with on each side one sensor and the magnetic bearings.

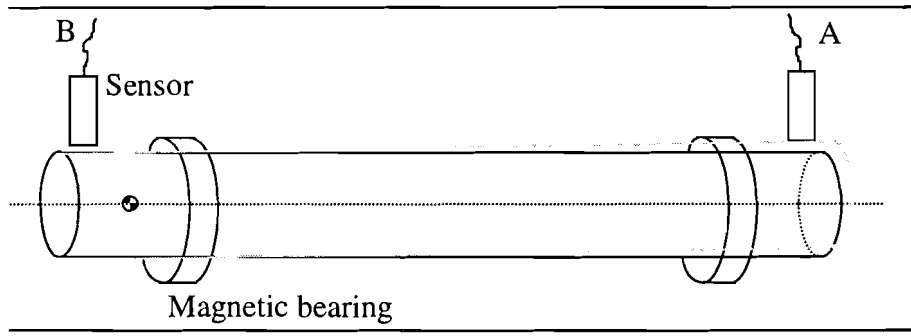

Figure 4-11, non collocation of sensor and bearing

Because of the non-collocation of the sensor and the actuator (magnetic bearing) a rotation point occurs between both of them (indicated at the B-side of the shaft). This rotation is modelled by the extra pole/zero-pairs and is an unstable phenomena. The instability is prevented because the shaft is magnetically borne on the other side.

4.4 The identification

Sixteen transfer functions should be measured, to reduce this, the black box modelling is changed to grey box modelling which means that the knowledge of the plant is used for the identification. Known from the white box model, when the shaft is not rotating, only a direct coupling between the current and the displacement and a cross coupling exists. The transfer function for the cross coupling (see Figure 4-12) is equal to the transfer function for the direct coupling besides a constant gain. So, a force f_{xa} on one side of the shaft will result in a force f_{xb} on the other side of the shaft (the cross coupling).

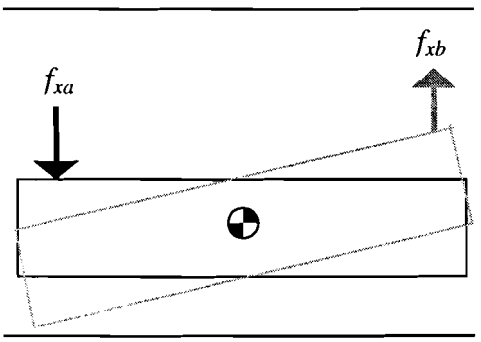

Figure 4-12, cross coupling

When the shaft is rotating, also the gyroscopic couplings have the same transfers, now besides a speed dependent gain and one zero (at one on the real axis) extra. This extra zero is not found in the frequency responses measured in section 4.3.1.

The identified model will only be valid for a non-rotating shaft. The coupling between the x- and y-axis, which would be theoretically zero, is modelled as a gyroscopic coupling. The controller that will be designed later on will be robust enough to handle rotating shafts.

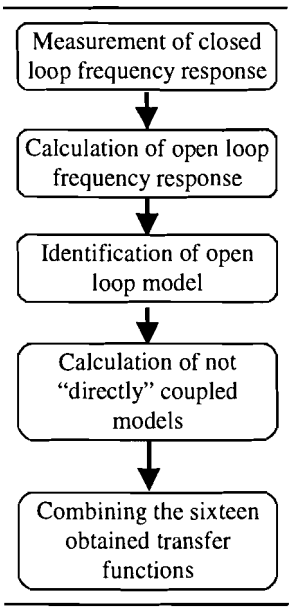

Figure 4-13, identification scheme

The complete identification is done as described in Figure 4-13. First a measurement of the frequency responses in closed loop is done, closed loop is here the relation between $r_2(t)$ and $y(t)$. Since the controller is known, the open loop model of the plant can be calculated with the use of Appendix D. After this point the identification can be started.

The identification is done in the frequency domain. This means the identification algorithm tries to find a model (with given number of poles and zeros) with a frequency response that fits the measured response as good as possible. The number of poles and zeros is chosen, based on the white box model and the steady state gain is corrected. There are no zeros and two poles modelled. The bending modes of the shaft, these were not modelled in the white box model, are left out. The controller should suppress these modes.

The not "directly coupled" transfer functions, meaning the coupling within the bearings and within the plane, can be calculated by using the direct coupled transfer function and

introducing in this transfer function a certain gain. The dynamics of the shaft are assumed to be equal for direct and not directly coupled transfers, only the gain is different. E.g. when one end of the shaft is moved upwards the shaft on the other side will move downwards, the shaft rotates. This means that the gain for the coupling within the plane is negative compared to the gain for the direct coupling.

Finally the sixteen transfer functions are combined to one discrete state space representation.

4.5 Validating the identification results

A first validation can be done by checking the two identified poles, if they are both unstable or stable the identification was not correct. Known from the white box model, one should be stable and one should be unstable and they all should be approximately mirrored in the imaginary axis (s-domain).

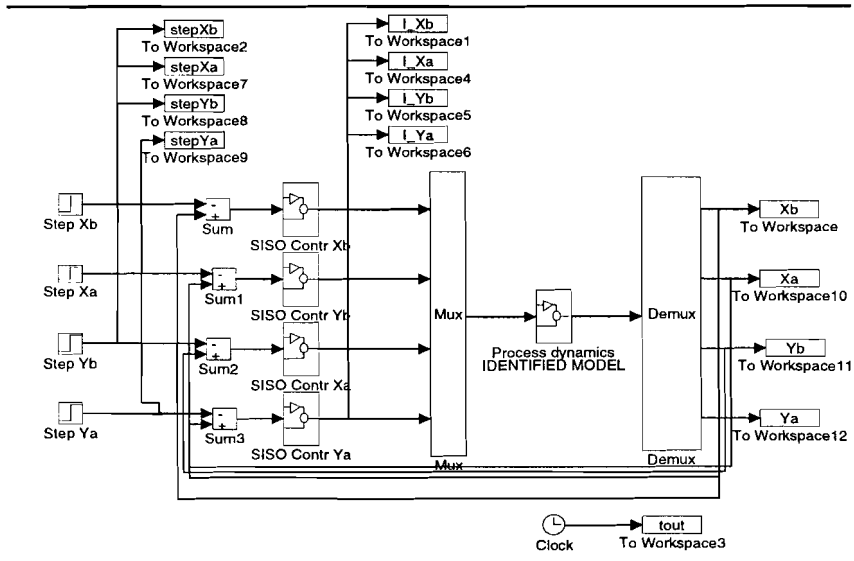

Figure 4-14, simulink model for validation

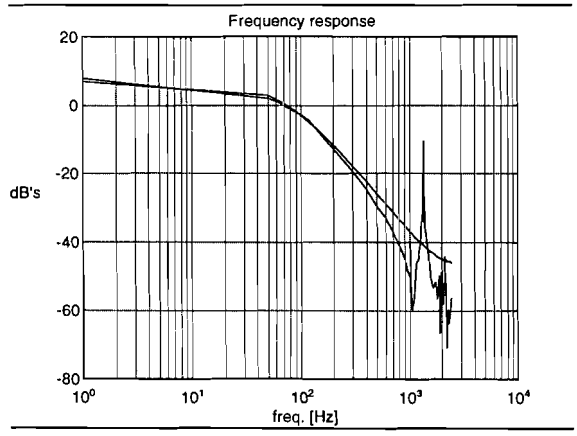

Figure 4-15, fit of corrected freq. response

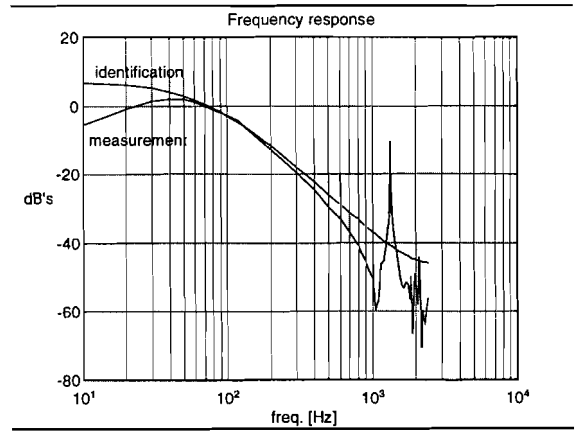

Figure 4-16, fit of frequency response

Also the frequency responses can be compared. In Figure 4-15 and Figure 4-16 the frequency responses used for the identification are given and the result of the identification. In Figure 4-15 the identification result is given together with the measurement. In this measurement the

gain for the steady state is changed. In Figure 4-16 the real measurement is given and again the previous done identification. The additive error, see Figure 5-8, is for low frequencies bigger when the steady state is not changed.

Since the process is open-loop unstable the obtained models by identification can only be validated in a closed-loop system. For this reason the models are included in a Simulink file (see Figure 4-14). The step responses of the Simulink model and the measured step responses are compared to each other.

First the step responses of the direct coupling are described. The results for each of these four responses is approximately the same, so only one response is given in Figure 4-17. The main difference that is found is the oscillation in the simulated model. This effect is absent by the occurrence of Eddy-currents in the real plant, which introduce a certain damping. This is a non-linear effect and can not be linearly .odelled. The amplitude and the settling time are approximated well.

However, more important is that this damping is mainly caused by the two pole/zero-pairs that could not be modelled. To answer the question if it is a problem when these two pole/zero-pairs are not modelled there should be anticipated on chapter 5. The controller that will be developed is a H_∞-controller. The development of such a controller is done in the frequency domain. In this domain the two pole/zero-pairs could not be traced. Every order of the identified plant will return in the controller. So, including the two pole/zero-pairs will raise the order of the controller and will not raise the performance of the controller.

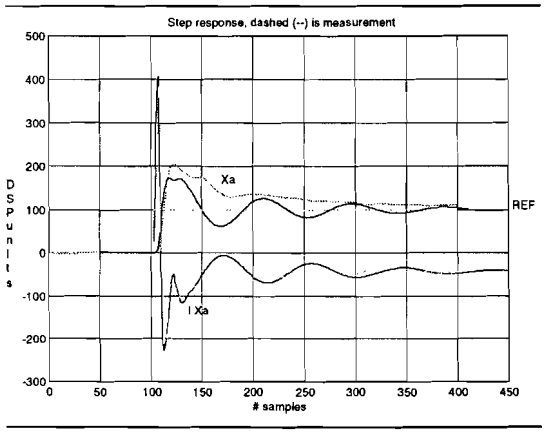

Figure 4-17, validation of direct coupling

The not-direct couplings are identified for the non-rotating case. The gains can become higher for a rotating shaft, the controller to be designed should be robust enough to handle this. In Figure 4-18 a step response is given for one of the inputs $r_2(t)$ and all four outputs. The results of the identifications are approximating the shaft and its dynamics good.

The extra zero in the gyroscopic coupling is left out since it gave worse results and could not be traced in the frequency response. The transfer functions becomes finally:

	Output X_a	Output Y_a	Output X_b	Output Y_b
Input X_a	$\frac{-0.0083}{-0.4264z^2+0.8174z-0.3873}$	$\frac{-6.6134e-4}{-0.4264z^2+0.8174z-0.3873}$	$\frac{0.0019}{-0.4264z^2+0.8174z-0.3873}$	$\frac{1.4880e-4}{-0.4264z^2+0.8174z-0.3873}$
Input Y_a	$\frac{-5.9639e-4}{-0.4318z^2+0..8175z-0.3809}$	$\frac{-0.0099}{-0.4264z^2+0.8174z-0.3873}$	$\frac{1.3916e-4}{-0.4318z^2+0..8175z-0.3809}$	$\frac{0.0019}{-0.4318z^2+0..8175z-0.3809}$
Input X_b	$\frac{0.0012}{-0.4257z^2+0.8174z-0.3881}$	$\frac{3.1030e-5}{-0.4257z^2+0.8174z-0.3881}$	$\frac{-0.0078}{-0.4257z^2+0.8174z-0.3881}$	$\frac{-2.3273e-4}{-0.4257z^2+0.8174z-0.3881}$
Input Y_b	$\frac{2.7583e-4}{-0.4723z^2+0.8148z-0.3360}$	$\frac{0.0035}{-0.4723z^2+0.8148z-0.3360}$	$\frac{-0.0010}{-0.4723z^2+0.8148z-0.3360}$	$\frac{-0.0125}{-0.4723z^2+0.8148z-0.3360}$

Finally it is nice to compare the identification results with the mathematical results.

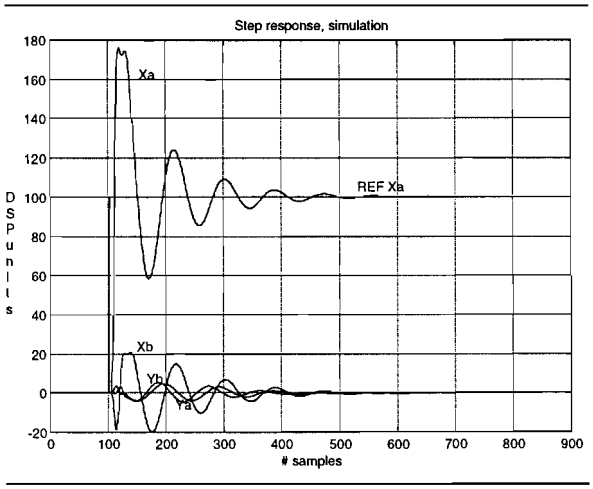

Figure 4-18, simulation of the couplings

When from both a bode diagram is plotted, see Figure 4-19, it can be seen that they are almost equal to each other.

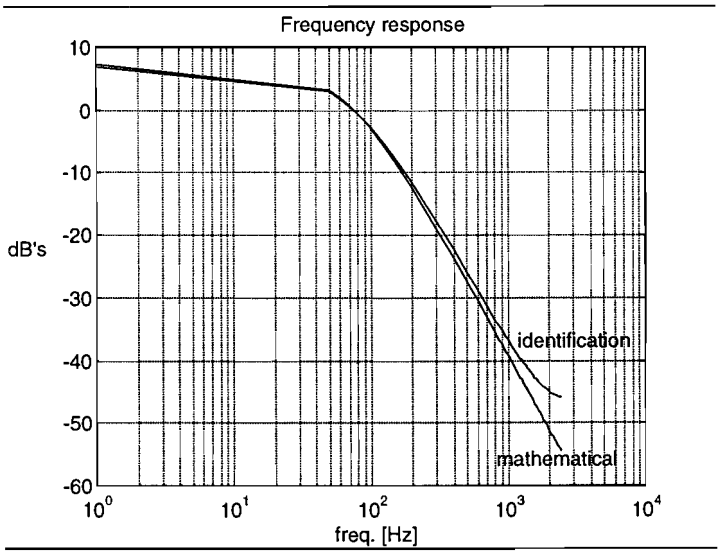

Figure 4-19, frequency response of mathematical description and identification

5. MIMO-controller development for the AMB

The controller to be designed for the AMB should be robust enough to handle loading of the shaft with small masses and high-speed rotations. In an attempt to improve the controller delivered by MECOS Traxler AG the design of a MIMO controller is chosen. In the previous chapters it is already made clear that couplings occur between the different planes (indirect couplings within the bearing and within the plane). These couplings can be suppressed using MIMO-control. To obtain good robustness of the closed loop system, H_∞-controller design is used.

Before the design of a MIMO-controller is started first four SISO H_∞-controllers are designed, the development of these controllers is described in section 5.4. After this the MIMO-controller is designed and the improvements are examined, this is done in section 5.5. First is started with the description of the tracking problem and the explanation of the weighting filters in section 5.1 and the description of the augmented plant in section 5.2.

5.1 The tracking problem

The closed loop system of Figure 4-1 is given once more in Figure 5-1, now slightly changed into a shorter form. Again, note the plus- and minus-signs.

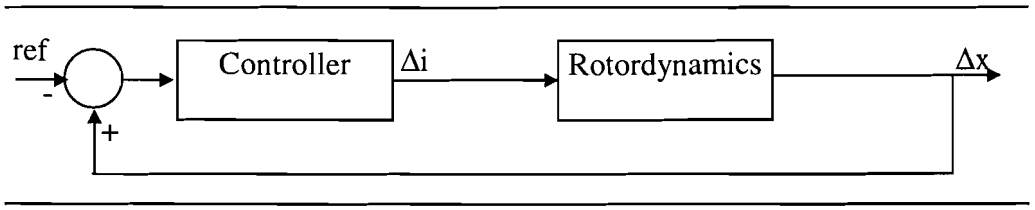

Figure 5-1, closed loop system

The plant is, as mentioned before, a MIMO system with four inputs and four outputs. Each output of the plant indicates the displacement (Δx) from the nominal value at one of the sensors. The inputs are the control currents (Δi) for the electromagnets. The controller to be designed, is fed with four error signals. These error signals are the difference between the displacements and the reference signals (*ref*). With these reference signals the shaft can be positioned in any direction. The controller has to make sure that the tracking is done as fast as possible. The modelled plant (see chapter 4) includes the actuators and the sensors.

The block diagram of Figure 5-1 should now be extended with weighting filters, see Figure 5-2. The use of weighting filters is of crucial importance to derive a controller, which satisfies the design objectives.

It should be mentioned that the process P(z) is given in the z-domain (discrete) and the controller to be designed should also be in the z-domain. Because of this all the input and output signals are defined in DSP units.

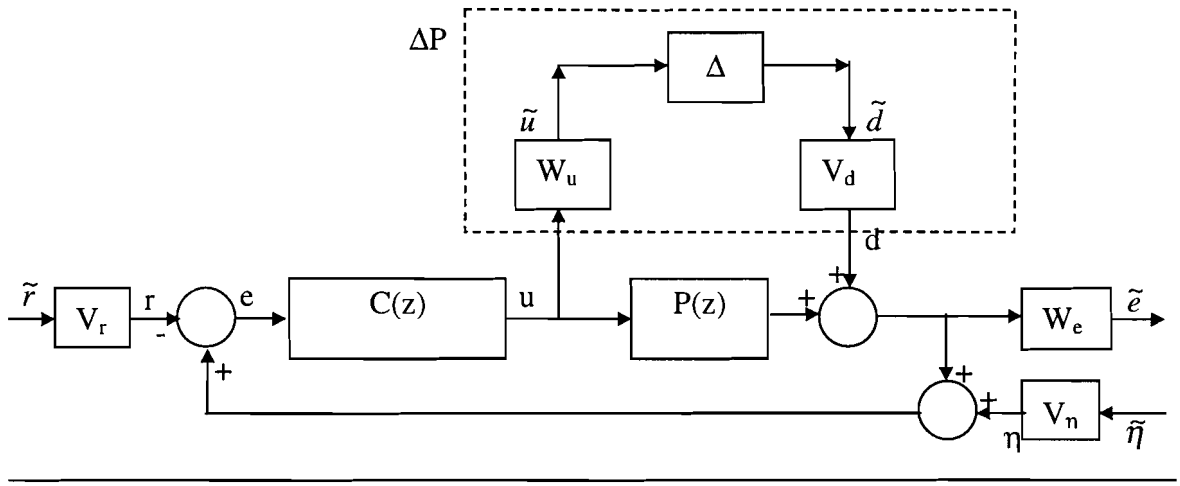

Figure 5-2, block diagram with weighting filters

The block ΔP represents the additive model perturbation. This ΔP is determined by:

- Limited identification: the identification done in the previous chapter is slightly different from the measurements.
- Unmodelled dynamics: the real behaviour of the system is approximated by a simple representation. For example the bending modes of the shaft are not modelled, also different loads and the rotation of the shaft are not modelled.
- Time variance: the real dynamics of the plant change in time due to, for instance, the influence of change in temperature. These effects are supposed to be very small.

The actual inputs, defined in Figure 5-2, are the outputs of the following input weighting filters:

V_r: the characterisation on the references, each frequency (up to the sample frequency) is allowed and so this weighting filter can be modelled as a constant with a value of 0dB. A constant value is chosen above a low pass to keep the order of the controller low.

V_η: the characterisation on the sensor noise. When the reference is set to zero the output of the sensor does have an uncertainty of +1 or -1 DSP unit. The total range is +2048 or –2048 DSP units. This filter is modelled with a constant value of -66dB.

V_d: the characterisation of the disturbance. This weighting filter should model the perturbation ΔP and the disturbances because of high-rotation speeds and loads on the shaft. Modelling the perturbation is done together with the weighting filter W_u.

The actual output signals are the input signals of the following output weighting filters:

W_u: the weighting filter to weight the actuator-input. This filter will also model the perturbation. More about this weighting filter is given in the sections 5.4 and 5.5.

W_e: the weighting filter to weight the output of the plant. The output should have a steady state error of zero and because of this the weighting filter should incorporate an integrator.

5.2 The augmented plant

Before a H_∞-controller can be designed, the first step is to set-up an augmented plant [DAM98], given in Figure 5-3. The plant is given for the MIMO system but there are no differences for the SISO case.

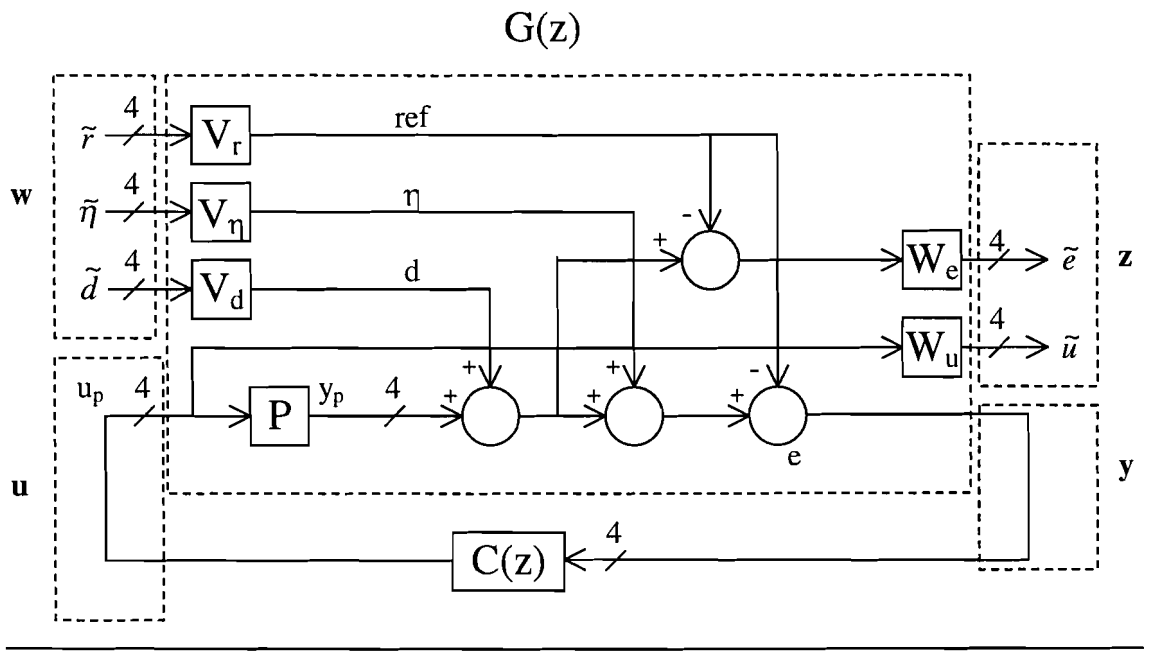

Figure 5-3, augmented plant

In the augmented plant are **w**, **z**, **y** and **u** vectors:

w: contains the exogenous inputs $\tilde{\eta}$, $\tilde{d}$ and $\tilde{r}$.

z: contains the output signals that have to be minimised.

y: contains the actually measured signals.

u: contains the output of the controller, which is alplied to the augmented system, described by G(z).

In the z-domain we may write the augmented plant in the following form:

$$\begin{pmatrix} \mathbf{z} \\ \mathbf{y} \end{pmatrix} = \begin{pmatrix} \mathbf{G}_{11} & \mathbf{G}_{12} \\ \mathbf{G}_{21} & \mathbf{G}_{22} \end{pmatrix} \begin{pmatrix} \mathbf{w} \\ \mathbf{u} \end{pmatrix}$$

while:

$$\mathbf{u} = \mathbf{C}\mathbf{y}$$

denotes the controller. Eliminating **u** and **y** yields to:

$$\mathbf{z} = \left[\mathbf{G}_{11} + \mathbf{G}_{12}\mathbf{K}(\mathbf{I} - \mathbf{G}_{22}\mathbf{K})^{-1}\mathbf{G}_{21}\right]\mathbf{w} = \mathbf{M}(\mathbf{K})\mathbf{w} .$$

The control aim requires:

$$\min_{\text{K stabilising}} \sup_{\mathbf{w}\in\mathcal{L}_2} \frac{\|\mathbf{z}\|_2}{\|\mathbf{w}\|_2} = \min_{\text{K stabilising}} \|\mathbf{M}(\mathbf{K})\|_\infty . \qquad (5.1)$$

where

$$\|\mathbf{s}\|_2 = \sqrt{\int_0^\infty |s(t)|^2 dt}$$

is the two norm, which expresses the power of energy of the signal *s(t)*. $£_2$ is a set of signals:

$$£_2 = \left\{\mathbf{s}:\mathbf{T}\to\mathbf{W}\,\middle|\,\|\mathbf{s}\|_2 < \infty\right\}.$$

When a signal *s(t)* belongs to $£_2$ then its power or energy is bounded.

The interpretation of the left side of equation (5.1) is as follows:

Above all, there has to be found a stabilising controller C. In this equation "$\sup_{\omega\in£_2}$" indicates that **w** is a worst disturbance, which is however bounded. For this worst disturbance, the energy of **z**, which contains the actuator input and the output error, should be minimised.

From the augmented plant in Figure 5-3 we can determine:

$$\begin{pmatrix}\tilde{e}\\ \tilde{u}\end{pmatrix} = \begin{pmatrix} -W_e(I-PC)^{-1}V_r & W_ePC(I-PC)^{-1}V_\eta & W_e(I-PC)^{-1}V_d \\ -W_uC(I-PC)^{-1}V_r & W_uC(I-PC)^{-1}V_\eta & W_uC(I-PC)^{-1}V_d \end{pmatrix}\begin{pmatrix}\tilde{r}\\ \tilde{\eta}\\ \tilde{d}\end{pmatrix},$$

which gives a closed loop transfer matrix **M**:

$$\mathbf{M} = \begin{pmatrix} \frac{\tilde{e}}{\tilde{r}} & \frac{\tilde{e}}{\tilde{\eta}} & \frac{\tilde{e}}{\tilde{d}} \\ \frac{\tilde{u}}{\tilde{r}} & \frac{\tilde{u}}{\tilde{\eta}} & \frac{\tilde{u}}{\tilde{d}} \end{pmatrix} = \begin{pmatrix} -W_e(I-PC)^{-1}V_r & W_ePC(I-PC)^{-1}V_\eta & W_e(I-PC)^{-1}V_d \\ -W_uC(I-PC)^{-1}V_r & W_uC(I-PC)^{-1}V_\eta & W_uC(I-PC)^{-1}V_d \end{pmatrix}$$

If we can manage to obtain:

$$\|M\|_\infty < \gamma \approx 1$$

then it can be guaranteed that:

$$\forall\omega\in\Re: \begin{pmatrix} \left|(I-PC)^{-1}\right| < \frac{1}{|W_eV_r|} & \left|PC(I-PC)^{-1}\right| < \frac{1}{|W_eV_\eta|} & \left|(I-PC)^{-1}\right| < \frac{1}{|W_eV_d|} \\ \left|C(I-PC)^{-1}\right| < \frac{1}{|W_uV_r|} & \left|C(I-PC)^{-1}\right| < \frac{1}{|W_uV_\eta|} & \left|C(I-PC)^{-1}\right| < \frac{1}{|W_uV_d|} \end{pmatrix}.$$

Now the closed loop transfers can be shaped by an appropriate choice of the weighting filters. Which filters can be used for shaping the sensitivity, the complementary sensitivity and the control sensitivity can be seen in equation (5.2). The real closed loop system contains no weighting filters.

$$\forall\omega\in\Re: \begin{pmatrix} |S| < \frac{1}{|W_eV_r|} & |T| < \frac{1}{|W_eV_\eta|} & |S| < \frac{1}{|W_eV_d|} \\ |R| < \frac{1}{|W_uV_r|} & |R| < \frac{1}{|W_uV_\eta|} & |R| < \frac{1}{|W_uV_d|} \end{pmatrix} \tag{5.2}$$

where S denotes: Sensitivity

T denotes: Complementary sensitivity

R denotes: Control sensitivity

5.3 Control goals and constraints

The control block C(z) has to be designed in such way that the reference is tracked as fast as possible. To achieve this an optimal form should be found between the control goals and constraints:

1. Stability — the closed loop system should be stable.
2. Tracking — the output of the plant should follow the reference signal as good as possible.
3. Disturbance reduction: — the influence of disturbance d should be small.
4. Sensor noise reduction: — the noise η introduced by the sensor should not affect the output of the process much.
5. Avoidance actuator saturation: — the actuator should not become saturated.
6. Robustness: — if the dynamics of the process change, the performance of the system should stay the same.

Each of these six points will be described in the following sections.

5.3.1 Stability

The closed loop system is required to be stable. Any finite disturbance somewhere in the closed loop may not cause other signals in the loop to become infinite. All transfers from inputs to outputs have to be checked on possible unstable poles. This means that unstable modes have to be reachable from **u** to guarantee the existence of a stabilising controller. The unstable modes also have to be observable from **y**. When the controller is designed a second order model is used, this means the model without two pole/zero pairs caused by the non-collocation of the sensor and actuator. The controllers designed will stabilise the model used as well as the real system since the instability is prevented because the shaft is magnetically bored on the other side (see section 4.3.3).

5.3.2 Tracking

The output of the plant, better said the displacement, can be set to any value within a given range by the reference signal. The output of the plant should track this reference exactly, within a given bandwidth. To track the reference signal exactly the controller should have an integrator to achieve a steady state error of zero.

5.3.3 Disturbance reduction

The disturbance reduction has to be large at low frequencies, since there should be achieved a zero steady state error and is allowed to be lower for high frequencies. Generally spoken, it is preferred to make this reduction band as wide as possible to achieve the fastest responses.

5.3.4 Sensor noise reduction

To decrease the influence of the sensor noise a controller should be designed in such way that the transfer from the sensor noise η to the output e (complementary sensitivity) is small in the frequency band where η is most disturbing.

5.3.5 Actuator saturation avoidance

It is necessary that the actuator is not saturated. A resistor and an inductance can approximate the coil of the electromagnet, see Figure 5-4.

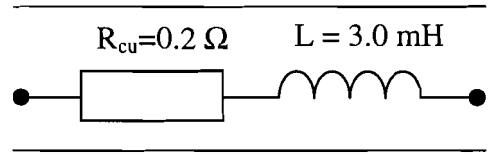

Figure 5-4 , coil of electromagnet

The maximum current I_{max} = 6 [A]. The cut-off frequency ω_g is given by

$$\omega_g = \frac{R_{cu}}{L} = 66\,[\text{rad/s}].$$

The premagnetization current i_0 is typically only a part of the maximum current I_{max}, for the practical set-up i_0=0.4I_{max}.

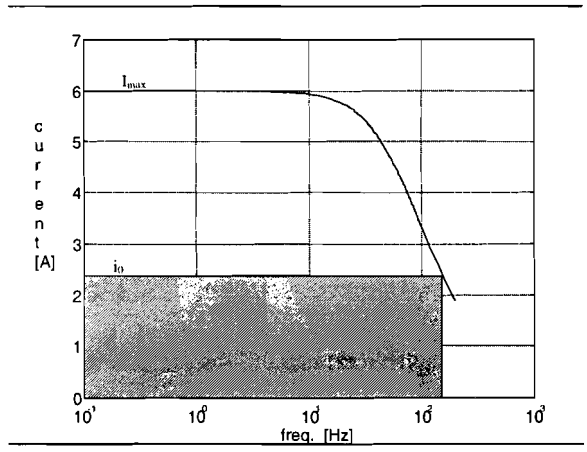

Figure 5-5, frequency response of actuator

In Figure 5-5 can be seen that the operation range of the actuator is about 150 Hz, after this the damping is 20dB per decade.

5.3.6 Robustness

The controller to be designed should be robust for the uncertainty block ΔP, modelling the additive perturbations. According to the small gain theorem the system of Figure 5-6 is asymptotically stable if:

$$\|M\Delta P\|_\infty = \|R\Delta P\|_\infty < 1,$$

it is assumed here that R, the control sensitivity, is equal to M. This is true for additive perturbations.

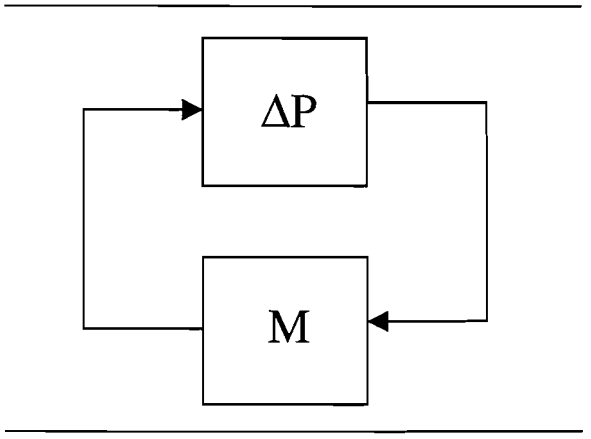

Figure 5-6, closed loop with additive perturbations

If we assume that C(z) stabilizes the nominal plant P(z) then the closed-loop system is stable for all aditive stable perturbations ΔP if:

$$\forall \omega \in \Re : |\Delta P(j\omega)| < \frac{1}{|R(j\omega)|}$$

5.4 SISO-controller design

Before a MIMO-controller is designed, four separate SISO controllers are designed. For each of these controllers the weighting filters are designed separately and the controller is calculated. Since the procedure is for each of the four controllers the same, only one controller design is described here. It will be the controller that should stabilise the displacement at x_a.

5.4.1 Weighting filters

The weighting filters V_r and V_η are already described in section 5.1 and are both set to a constant value.

The weighting filter W_e should weight the error (without sensor noise). Since the steady state error is preferred to be zero it should characterise an integrator. To overcome numerical errors during the calculation of the controller the gain of the filter should be constant for very low frequencies. The weighting filter is shown in Figure 5-7.

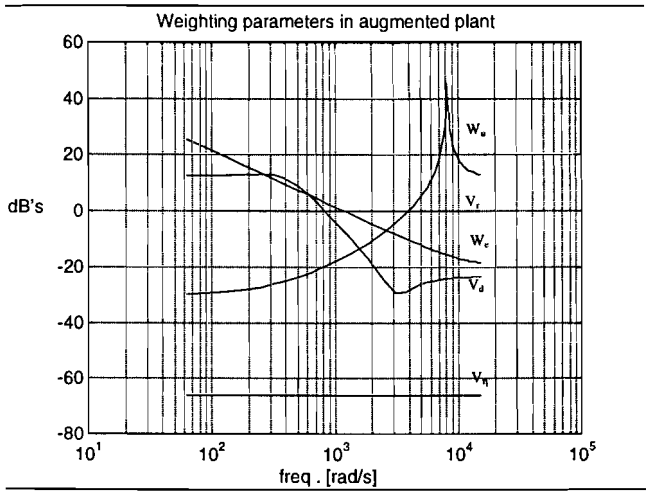

Figure 5-7, weighting filters

The actuator saturation is characterised by the weighting filter W_u. In section 5.3.5 it is already given that the saturation frequency is about 150 Hz. The weighting filter should be a high-pass filter with the cut-off frequency near 150 Hz, the filter is designed as a second order filter and is also shown in Figure 5-7. A second order filter was necessary to suppress the resonance frequency of the first bending mode.

Finally, the weighting filter V_d should model the perturbations of the plant together with W_u. V_d is chosen in such a way that the ΔP is covered, see Figure 5-8. Also this filter, here modelled as second order filter, is given in Figure 5-7. For low frequencies the perturbation ΔP is not covered since this ΔP is not valid because of measurement and calculation errors, see section 4.5.

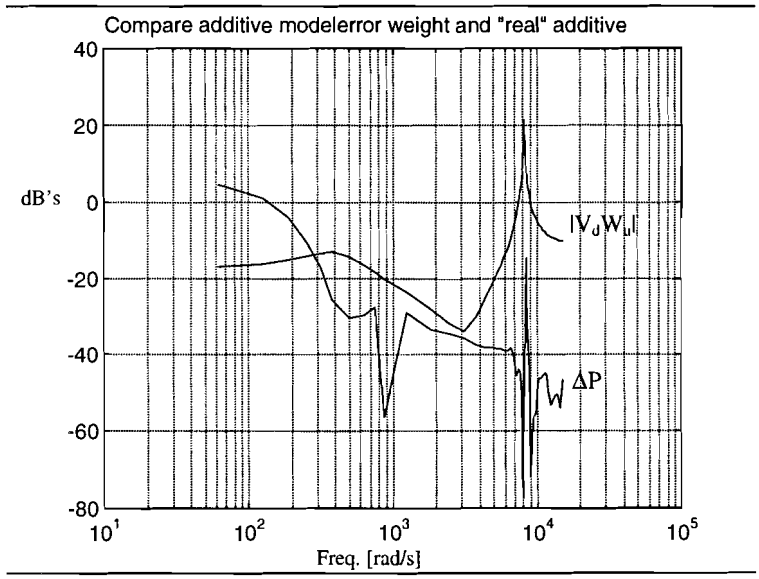

Figure 5-8, covering of process perturbations

5.4.2 Closed loop performance

With the weighting filters from the previous sub-section a controller is computed using the LMI toolbox of Matlab, a gamma close to 1 was found:

$$\gamma = 1{,}1 \; .$$

The sensitivity and the complementary sensitivity together with their bounds are given in Figure 5-9. The dotted lines in this figure denote the constraints, given by the choice of the weighting filters. The solid lines are the transfers of the closed loop system without weighting filters. These lines have to lie below the dotted lines, according to equation [5.2].

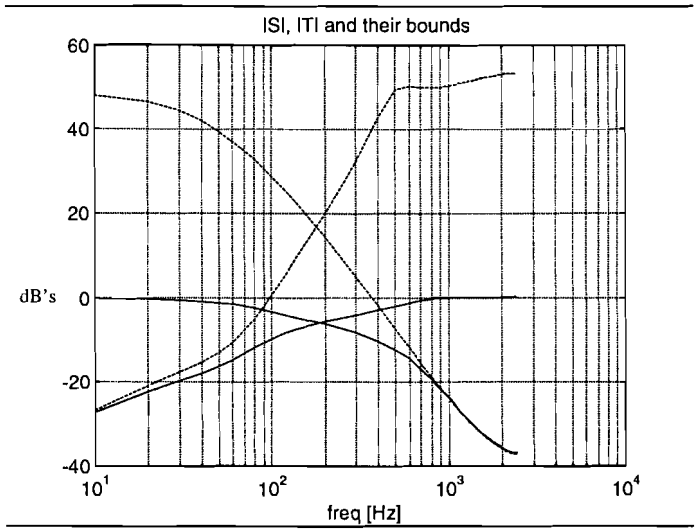

Figure 5-9, sensitivity and complementary sensitivity

The bode plot of the controller is given in Figure 5-10. Most remarkable is that the complete bode plot is above 0dB, even for the resonance peak. However, the closed loop gain at the resonance frequency is below 0dB. The integrating action of the controller can be seen quite clear.

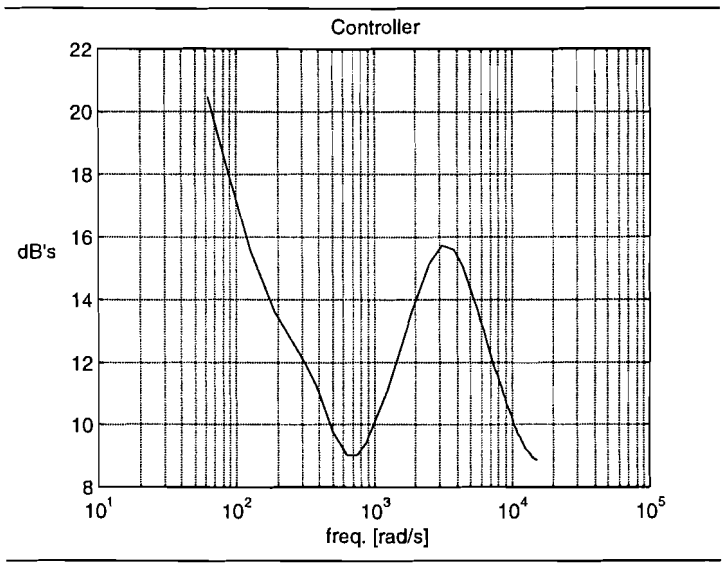

Figure 5-10, calculated controller

The controller is included in the Simulink[II] file and in the real system. A step response, see Figure 5-11, on both of these shows an amazing profit in performance. In the simulation as well as in the measurement the step response has become about three times faster (solid lines) than the controllers of MECOS Traxler AG (dashed lines), of course this is partly reached by demanding more from the actuator. However this seemed to be no problem.

[II] Simulink (a Matlab-toolbox) is copyrighted by The MathWorks inc.

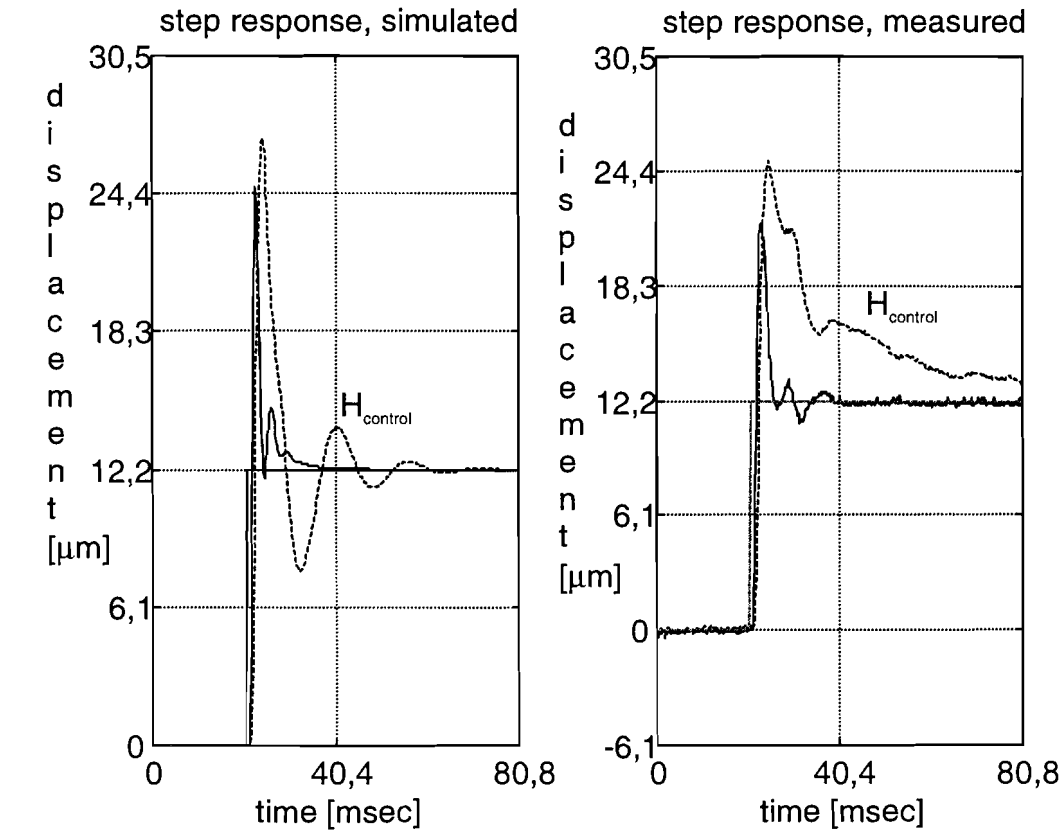

Figure 5-11, step responses

When all four controllers are designed in this way and implemented on the real shaft the process was unstable, since each of the controllers is very fast and they are both doing the same job. This can be explained with Figure 5-12.

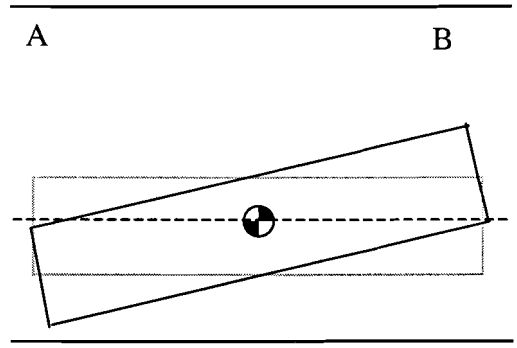

Figure 5-12, Unstable caused by using two SISO controllers

When the shaft is slightly rotated (black lines) and the reference is set to zero, (the shaft should be in horizontal position) the controllers should pull the shaft into the correct position. Since each controller is designed separately each controller will do its own job, this means that the controller at the A-side will pull the shaft up and the controller at the B-side will pull the shaft downwards. When the shaft at the A-side is pulled up, the shaft on the B-side will automatically go downwards (coupling within the plane, see section 3.3), the controller on the B-side is also pulling the shaft downwards. Now it can be sensed that pulling down the shaft on the B-side and up on the A-side is both going to fast, so the shaft goes beyond the horizontal position, which will destabilise the process.

To overcome this problem all four controllers are designed at the same time, a simple block diagram is given in the Figure 5-13.

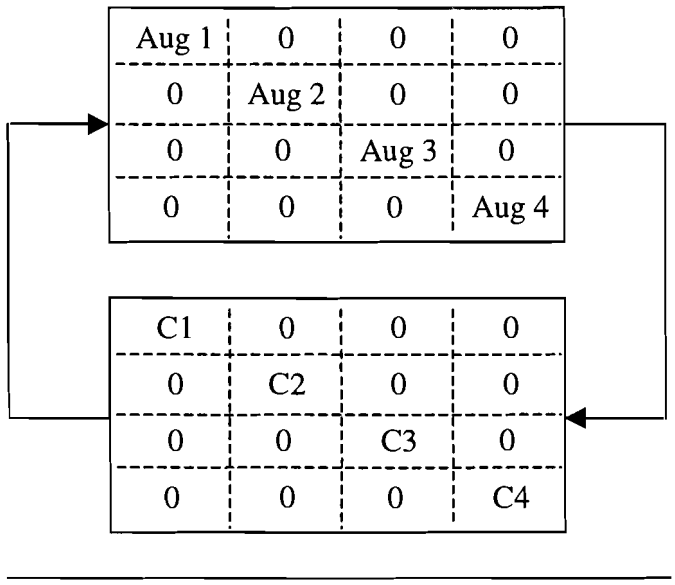

Figure 5-13, combining the augmented plants

Now all four of the augmented plants are combined. Again only the direct transfers are included in the augmented plant. With this structure the calculated controller is forced to have only elements on the diagonal, meaning that only the direct couplings are controlled. The question is now whether there is any difference in the controllers calculated one by one or all at once. It can be shown that the gamma that is calculated with the structure above will be at least equal or bigger then the worst gamma that was achieved when the controllers were calculated one by one, assuming that the same weighting filters were used. Even now the system was not stable when implemented.

To solve this problem two options are available. The first one makes use of an iterative process. For this the augmented plant should be changed slightly, now the complete MIMO structure should be available in the augmented plant. In case of the AMB three of the four SISO controllers should be implemented, e.g. the ones of MECOS Traxler AG. Now the fourth controller should be calculated based on H_∞-controller design. After the calculation of this controller this one should be implemented and the next controller should be removed and calculated again. This should be repeated at least once for each of the four controllers and there can be stopped when the controllers have converged to their final value.

Furthermore, there could be searched in the literature for the design of SISO controllers for MIMO systems. Probably there has been written some articles about this subject, hopefully the described techniques can be implemented easily in the software now available for calculating H_∞-controllers.

5.5 MIMO-controller design

Even though a MIMO controller can not be implemented, a MIMO controller is designed and simulated. The results were quite promising. To be more precise, two different MIMO controllers were designed. When the hardware is extended also MIMO controllers can be implemented in the MECOS Traxler AG set-up. The structure of these controllers restricts that only a MIMO controller can be designed for two inputs and two outputs. Also a full

MIMO controller (four inputs and four outputs) is designed, but this can not be implemented on the real system. This section is, just like the previous one, first giving the weighting filters and after that the results and performance characteristics.

5.5.1 Weighting filters

As already said only a 2x2 MIMO controller can be designed because of the restrictions of the real process. The calculated 2x2 MIMO controller is also used for controlling the other two inputs and outputs. Because of this the weighting filters that covers $\sup_{\omega\in\Re}\overline{\sigma}(\Delta P(j\omega))$can be the same for the 2x2 MIMO controller as well as the 4x4 MIMO controller. The maximum singular values do not change when the process is examined with two inputs and outputs or four inputs and outputs.

The weighting filters V_r and V_η are already described in section 5.1.

The weighting filter W_e should again weight the error (without sensor noise). Since the steady state error is preferred to be zero it should characterise an integrator. The weighting filter is shown in Figure 5-14.

The actuator saturation is characterised by the weighting filter W_u. In section 5.3.5 is given the saturation frequency is about 150 Hz. The weighting filter should be a high-pass filter with the cut-off frequency near 150 Hz, the filter is designed as a second order filter and is also shown in Figure 5-14.

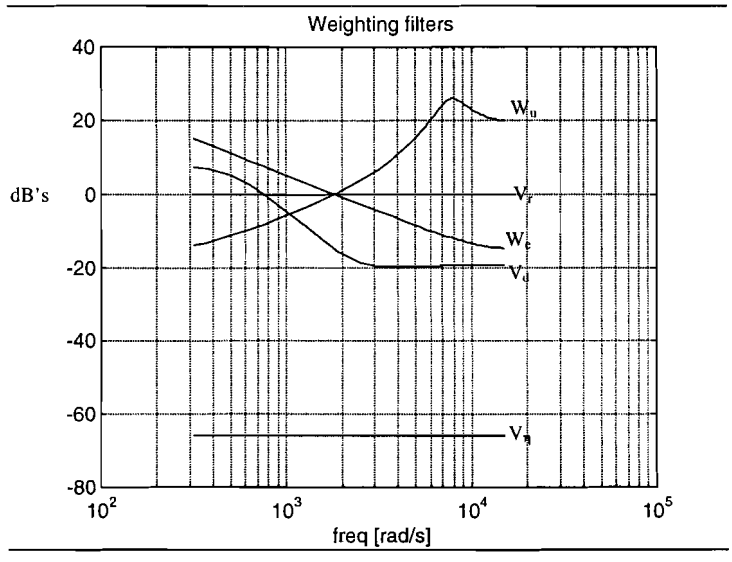

Figure 5-14, weighting filters

Finally, the weighting filter V_d should model the perturbations of the plant together with W_u. V_d is chosen in such a way that the $\sup_{\omega\in\Re}\overline{\sigma}(\Delta P(j\omega))$ is covered, see Figure 5-15. $\Delta P(j\omega)$ is in this case the MIMO process. Also this filter, here modelled as second order filter, is given in Figure 5-14.

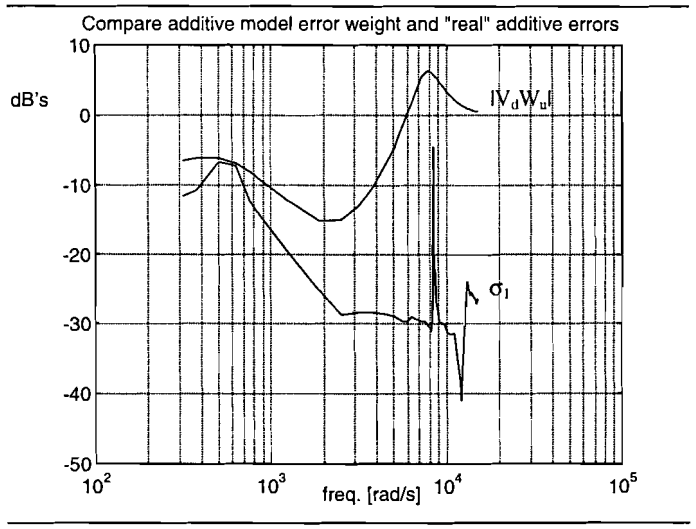

Figure 5-15, maximum singular value of P

5.5.2 Closed loop performance 2x2 MIMO controller

With the weighting filters from the previous sub-section a controller is computed using the LMI toolbox of Matlab, gamma was:

$$\gamma = 9{,}02\,.$$

The sensitivity and the complementary sensitivity together with there bounds are given in Figure 5-16. The dotted lines in this figure denote the constraints, given by the choice of the weighting filters. The solid lines are the transfers of the closed loop system without weighting filters. These lines have to lie below the dotted lines, according to equation [5.2]. In total their are plotted two sensitivities and two complementary sensitivities, one for the direct couplings and one for the indirect couplings.

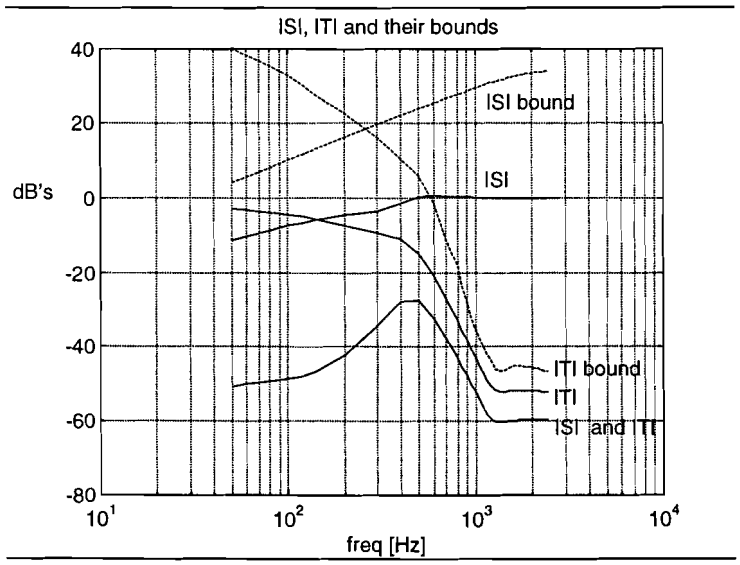

Figure 5-16, sensitivity and complementary sensitivity and their bounds

The intersection point of the boundaries is much above the 0dB point. This is caused by the fact that γ is not one, with the orders used for the filters it is not possible to lower the value of γ without changing the demands. So the robustness that would be achieved by the weighting filters is not reached. The intersection point of the real sensitivity and its complementary

sensitivity is below 0dB. This means that the performance can become even better, but then the robustness gets lower.

In Figure 5-17 two step responses are plotted. The reference for tracking the signal x_a is set to a displacement of 12,2 [µm] and the displacement is plotted. Also the indirect coupled displacement x_b is plotted. The dashed line gives the responses with the controller of MECOS Traxler AG and the solid lines the responses with the MIMO controller. It can be seen that the indirect coupling is reduced. The simulations are very promising and the implementation should give us the exact reductions of the indirect couplings.

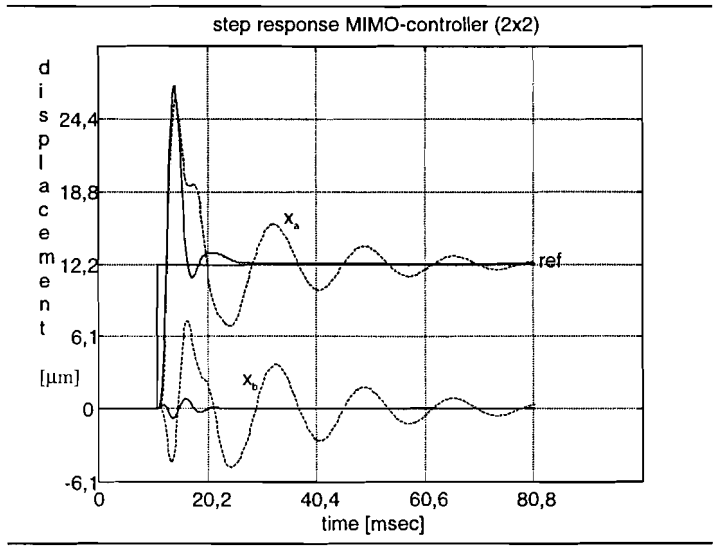

Figure 5-17, step response with two 2x2 MIMO controller

5.5.3 Closed loop performance 4x4 MIMO controller

With the weighting filters from sub-section 5.5.1 a controller is computed, gamma was:

$$\gamma = 9{,}11\,.$$

The sensitivity and the complementary sensitivity together with their bounds are given in Figure 5-18. The dotted lines in this figure denote the constraints, given by the choice of the weighting filters. The solid lines are the transfers of the closed loop system without weighting filters. These lines have to lie below the dotted lines, according to equation [5.2]. In four sensitivities and four complementary sensitivities are plotted, one for the direct couplings and three for the indirect couplings.

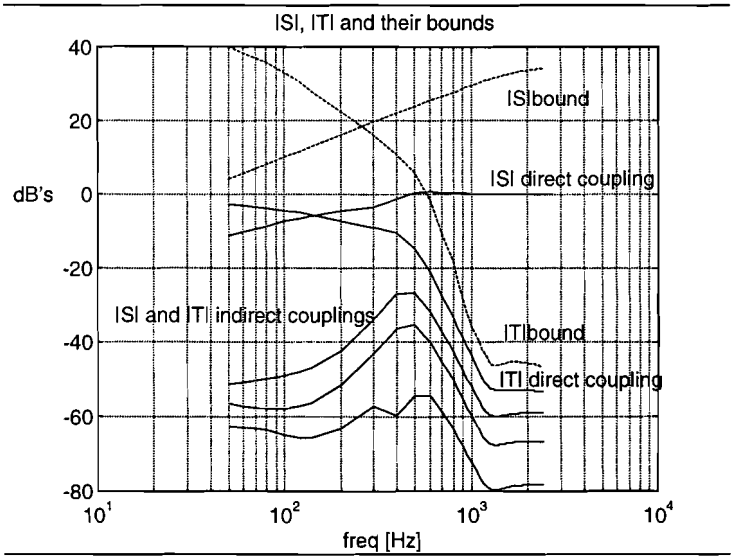

Figure 5-18, sensitivity and complementary sensitivity

For the performance and robustness is the same story valid as in sub-section 5.5.2. So also in this case the performance went down.

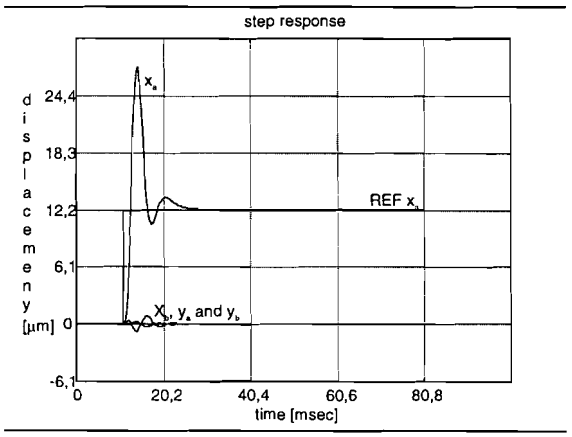

Figure 5-19, step response 4x4 MIMO controller

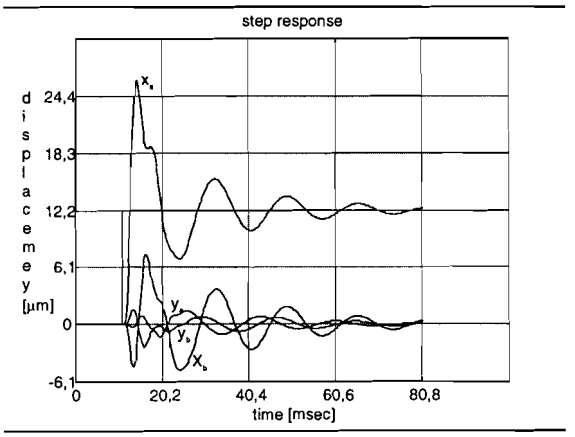

Figure 5-20, step response 4x SISO controller

Although the 4x4 MIMO controller can never be implemented, in Figure 5-19 the step response is plotted. The reference for tracking the signal x_a is set to a displacement of 12,2 [µm] and the displacement is plotted. Also the indirect coupled displacement x_b is plotted. In Figure 5-20 the responses with the controller of MECOS Traxler AG is plotted to compare with the MIMO controller. The indirect couplings are reduced, the difference between the couplings within the plane and within the bearing can not be recognised any more.

6. Conclusions and recommendations

This chapter will give an overview of the problems that were found, solutions to solve these and recommendations to improve the modelling and control of AMB system, this will be done in the next section. In section 6.2 a checklist is given which gives the most important things that should be taken into account when designing an AMB system.

6.1 Overview

Since AMB systems are not linear, unstable (without appropriate controllers) MIMO systems many problems occurs. These problems start occurring during the white box modelling, continues while doing identification and remains even when designing and implementing a robust controller. In the next paragraph is started with the white box modelling and after that the other problems and, if found, solutions are presented.

When a white box model is set-up for a non-linear system the question is for what purpose the model is used. If it is only used to get a feeling for the system it is enough to use a linearised mathematical description. During this graduation time it was enough to use a linearised mathematical description, the problems that occurred here were the little knowledge about the practical system. None of the variables like the length, mass or force/current characteristics was known or badly described in the technical specifications. Many of the parameters have to be guessed or calculated. Doing this, many uncertainties were introduced. However the model achieved seemed to approximate the identified and measured responses quite well. Most catching the eye was the two pole/zero pairs caused by he non-collocation of the sensor and the actuator, these could not be identified. To control the model with the controller available by MECOS Traxler AG was not possible. When the model will be used for more then just getting some feeling it is necessary to know more of the parameters of the AMB system. It can even be necessary to work with the non-linear mathematical description to design for example a non-linear controller or to validate the robustness of a developed controller. It is advised when a magnetic bearing system is designed to set up a useful non-linear mathematical description.

Since the AMB system is unstable the identification is also a bit harder then with stable systems. In this case an open-loop identification should be possible. The problem to identify in closed-loop is how to retrieve the open-loop unstable plant. When the identification is done in closed-loop and the transfer function of the plant is retrieved by calculating it from the knowledge of the transfer function of the controller and closed-loop system, some poles and zeros that should cancel each other will not because of noise. This can become a problem. This problem can be avoided when the open-loop is first calculated and then the identification is done. The best way to obtain a good model for an unstable MIMO system is to do a MIMO identification, for this all inputs should be excited at the same time. In the practical set-up used during this graduation project it was not possible. To obtain a better model then was achieved here the practical system should be extended in such a way that more inputs can be excited at the same time. It is also preferred that the signal generator in the practical set-up is replaced so more signals can be generated then just sinusoidal signals.

When a controller is designed a good model should be available to test the developed controllers. In the practical set-up from MECOS Traxer AG it was only possible to implement four SISO controllers, however the system could be extended with a MIMO controller (two inputs and two outputs). It is recommended according to the results that were achieved during the development of a MIMO controller to extend the system. Better results will then be

achieved, especially the indirect couplings will be suppressed a lot and this will make the system much faster. When designing a robust controller it is necessary to have knowledge about the sensors and actuators. Also here the technical specifications has it shortcomings. Perhaps with the nowadays prices of DSP's not logical, but if it is desired to design multiple SISO controller for a MIMO system it is needed to develop some iterative algorithm (see Appendix E) or search for articles written about this subject (see Appendix F).

A general conclusion can finally be that when a model should be set-up, black-box or white-box, for an unstable system or a robust controller should be designed it requires enough knowledge about the technical specifications.

6.2 Checklist

When an AMB-system is developed there should be paid attention to the following items:

- make sure that everything that can be known about the system is known, meaning knowing all the lengths, radiuses, masses, inertia's, characteristics (e.g. force-current characteristics), etc. ;
- set-up a very good mathematical description with the use of the knowledge above. This can be a non-linear description, valuable for testing robustness of the controller later on;
- while designing the AMB system it is worth to prevent non-collocation of sensors and actuators;
- design a very simple (e.g. PID) controller for the AMB-system, for closed-loop tests;
- do an identification of the system. Extend hardware, if necessary, to excite more then one input at a time and measure more samples;
- use the model obtained to design an appropriate controller and use the mathematical description to check its robustness and performance;
- implement the controller and test the complete set-up.

Bibliography

[BOE98] Boer, W. de
SOFTWARE MANUAL, FOR THE MINI VS: C3
University of Technology Eindhoven
Eindhoven (the Netherlands), 1998

[DAM98] Damen, A. and S. Weiland
ROBUST CONTROL
Draft version of August 19, University of Technology Eindhoven
Eindhoven (the Netherlands), 1998

[GAH95] Gähler, C. and R. Herzog
IDENTIFICATION OF MAGNETIC BEARING SYSTEMS.
Mathematical Modelling of Systems, Vol. 1 (1995), No. 1, p. 29-45.

[GAH97] Gähler, C., and M. Mohler, R. Herzog
MULTIVARIABLE IDENTIFICATION OF ACTIVE MAGNETIC BEARING SYSTEMS.
JSME International Journal. Series C, Mechanical Systems, Machine Elements and Manufacturing, Vol. 40 (December 1997), No. 4, p. 584-592.

[ROE90] Roest, R.
INLEIDING MECHANICA
Delft (the Netherlands), 3rd print 1990

[SCH94] Schweitzer, G. and H. Bleuler, A. Traxler
ACTIVE MAGNETIC BEARINGS: BASICS, PROPERTIES AND APPLICATIONS OF ACTIVE MAGNETIC BEARINGS.
Zürich (Swiss), 1994.

[VAN96] Vandenput, A.J.A.
ELECTROMECHANICA
Dictaatnr. 5794, University of Technology Eindhoven
Eindhoven (the Netherlands), 1996

Appendix A: Taylor-expansion

F_t is approximated by Taylor-expansion. It is assumed that $\Delta x << x_0$ and $\Delta y << y_0$. Furthermore the following first-order approximation is used

$$f(x_0 + \Delta x, y_0 + \Delta y) \approx f(x_0, i_0) + \Delta x \frac{\partial f(x_0, i_0)}{\partial x_0} + \Delta i \frac{\partial f(x_0, i_0)}{\partial i_0},$$

known as the Taylor-expansion. The derivation of the force F_t is as follows:

$$F = F_+ + F_-$$

$$F_t = K\left(\frac{i_0 + \Delta i}{x_0 - \Delta x}\right)^2 - K\left(\frac{i_0 - \Delta i}{x_0 + \Delta x}\right)^2$$

$$F_t = K\left\{\left(\frac{i_0 + \Delta i}{x_0 - \Delta x}\right)^2 - \left(\frac{i_0 - \Delta i}{x_0 + \Delta x}\right)^2\right\}$$

$$F_t \approx K\left\{\left[\left(\frac{i_0}{x_0}\right)^2 - \left(\frac{i_0}{x_0}\right)^2\right] + \Delta x\left[2\frac{{i_0}^2}{{x_0}^3} + 2\frac{{i_0}^2}{{x_0}^3}\right] + \Delta i\left[2\frac{i_0}{{x_0}^2} + 2\frac{i_0}{{x_0}^2}\right]\right\}$$

$$F_t \approx 4K\frac{{i_0}^2}{{x_0}^3}\Delta x + 4K\frac{i_0}{{x_0}^2}\Delta i$$

$$F_t = K_s \Delta x + K_i \Delta i$$

In the above derivation there can be seen that K_s is a quadratic function of the nominal current and K_i is a linear function of the nominal current.

Appendix B: motions and displacements

In Figure B-6-1 the three co-ordinate frames on the shaft are given on the left, in the middle the displacements by rotation around an angle β and on the right the displacements by rotation around an angle α.

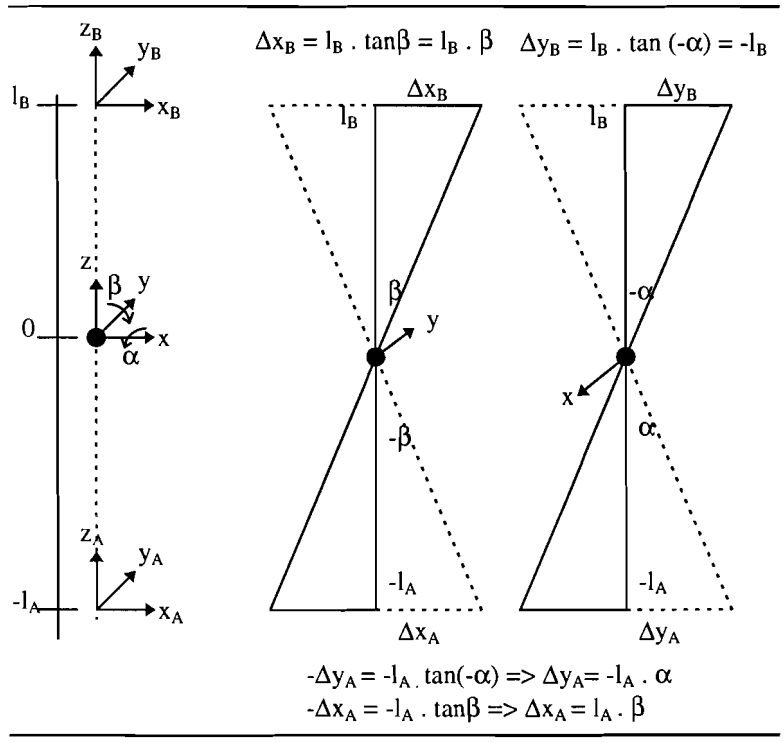

Figure B-6-1, displacements because of rotation

When there is a rotation around the y-axis with an angle β there will be a displacement Δx_B and Δx_A. With the basic trigonometry ($\tan\alpha = \frac{\Delta x_B}{l_B}$) this displacement can be calculated. The same can be done for Δx_A.

When there is a rotation around the x-axis by an angle α the displacement will go to the negative part of the y_B-axis. Since this is preferred to be positive the angle of rotation is chosen to be negative. Now again the displacements can be calculated with the basic trigonometry as done before.

In the calculations above it is assumed that the rotation angles are small, so the angles between Δx_j and l_j , $j \in \{A,B\}$ are approximately 90 degrees. This makes it possible to use the basic trigonometry as above.

Besides the rotations there can also be small translations. The four equations for the motion will then become:

$$x_B = \Delta x + \beta l_B$$
$$x_A = \Delta x + \beta l_A$$
$$y_B = \Delta y + -\alpha l_B$$
$$y_A = \Delta y + -\alpha l_A$$

Appendix C: Inertia

Momentum is calculated by:

$$J = \int r'^2 dm$$

The shaft can be approximated by 10 massif cylinders (Figure C-1).

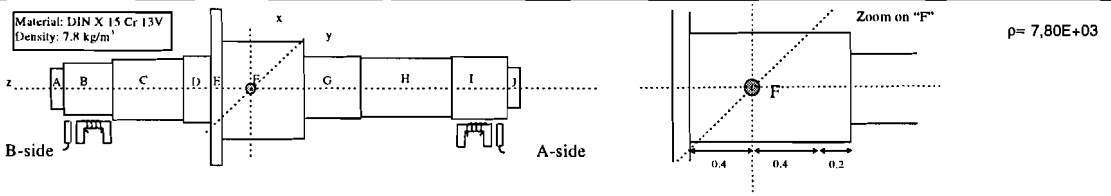

	diameter [m]	radius [m]	length [m]	volume [m^3]	mass [kg]	distance to centre of gravity	Jz [kg m^2]	Jx [kg m^2]	Jy [kg m^2]
A	29,50E-3	14,75E-3	13,00E-3	8,89E-6	69,31E-3	0,129688796	7,54E-6	1,17E-3	1,17E-3
B	30,50E-3	15,25E-3	42,50E-3	31,05E-6	242,20E-3	0,101938796	28,16E-6	2,55E-3	2,55E-3
C	31,50E-3	15,75E-3	44,00E-3	34,29E-6	267,46E-3	0,058688796	33,17E-6	964,38E-6	964,38E-6
D	46,00E-3	23,00E-3	11,50E-3	19,11E-6	149,07E-3	0,039561204	39,43E-6	234,95E-6	234,95E-6
E	82,00E-3	41,00E-3	7,00E-3	36,97E-6	288,34E-3	0,021688796	242,35E-6	136,82E-6	136,82E-6
F	46,00E-3	23,00E-3	45,00E-3	74,79E-6	583,33E-3		154,29E-6	109,28E-6	109,28E-6
G	31,00E-3	15,50E-3	29,00E-3	21,89E-6	170,73E-3	0,041311204	20,51E-6	303,33E-6	303,33E-6
H	30,40E-3	15,20E-3	58,50E-3	42,46E-6	331,20E-3	0,085061204	38,26E-6	2,49E-3	2,49E-3
I	30,50E-3	15,25E-3	45,00E-3	32,88E-6	256,45E-3	0,136811204	29,82E-6	4,84E-3	4,84E-3
J	29,50E-3	14,75E-3	13,00E-3	8,89E-6	69,31E-3	0,165811204	7,54E-6	1,91E-3	1,91E-3
total:			308,50E-3	311,20E-6	2,43E+0		601,08E-6	14,71E-3	14,71E-3

distance to sensor (B-side):	117,5E-3 [m]
distance to sensor (A-side):	151,8E-3 [m]
distance to bearing (B-side):	96,2E-3 [m]
distance to bearing (A-side):	130,8E-3 [m]

Measurement: mass about 2.8kg, this includes the coils!!!!!

Figure C-1, shaft dimensions and some calculations

The volume of the complete shaft is approximately 301.10^{-6} m^3 and the material is DIN X 15 Cr 13 V, 1.4024 (HC510). This makes a mass of 2.43 kg. To calculate the inertia J_z the cylinder is divided into a large number of thin-walled cylinders, fitting in each other, with a radius s and thickness ds. The mass of one such cylinder is:

$$m_s = \rho 2\pi s l ds$$

The complete inertia will then be, after integration over the radius:

$$J_z = \tfrac{1}{2} mR^2$$

The inertia J_x and J_y, which are equal because the shaft is symmetric, can be calculated by

$$J_x = \tfrac{1}{12} ml^2 + ms^2 .$$

Where m is the mass of the cylinder, l is the length of the cylinder and s is the distance from the centre of one cylinder to the centre of mass.

The length from the centre of gravity to the magnetic bearing on the B-side is 96.2mm and to the magnetic bearing on the A-side 130.8mm. The length from the centre of gravity to the sensors on the B-side is 117.6mm and to the sensor on the A-side 151.8mm. These lengths are all read from the manual of the miniVS, C3.

Appendix D: Transfer functions for the identification

In Figure D-1 the block diagram of the complete AMB-system is given. It should be mentioned that the rotordynamics block does include the power-amplifier and the sensors. Both of them have such a wide bandwidth that their dynamics can be neglected here.

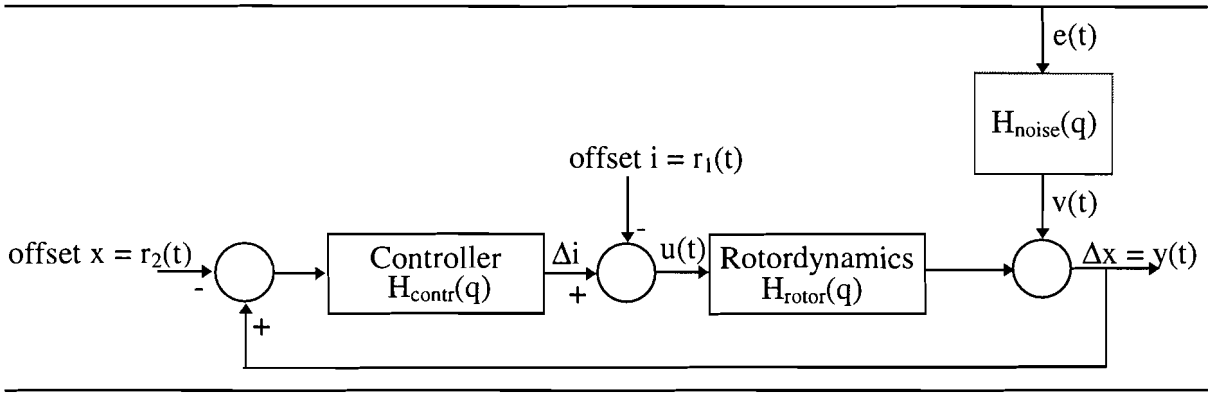

Figure D-1, block diagram

The output is equal to:

$$\begin{aligned} Y(j\omega) &= H_{rotor}(j\omega)\,U(j\omega) + V(j\omega) \\ &= H_{rotor}(j\omega)\,U(j\omega) + H_{noise}(j\omega)E(j\omega) \\ &= H_{rotor}(j\omega)\,H_{contr}(j\omega)\big(Y(j\omega) - R_2(j\omega)\big) - H_{rotor}(j\omega)\,R_1(j\omega) + H_{noise}(j\omega)\,E(j\omega) \end{aligned}$$

This makes the transfer:

$$Y(j\omega)\big(1 - H_{rotor}(j\omega)\,H_{contr}(j\omega)\big) = -H_{rotor}(j\omega)\,H_{contr}(j\omega)R_2(j\omega)$$

$$Y(j\omega) = \frac{-H_{rotor}(j\omega)\,H_{contr}(j\omega)}{1 - H_{rotor}(j\omega)\,H_{contr}(j\omega)}R_2(j\omega)$$

$$H_{cl}(j\omega) = \frac{-H_{rotor}(j\omega)\,H_{contr}(j\omega)}{1 - H_{rotor}(j\omega)\,H_{contr}(j\omega)}$$

when $R_1(j\omega)$ is zero and the noise is neglected. The open-loop transfer can be calculated when H_{contr} is known.

$$H_{rotor}(j\omega) = \frac{H_{cl}(j\omega)}{H_{cl}(j\omega)\,H_{contr}(j\omega) - H_{contr}(j\omega)}$$

The output signal was already measured and the input signal can be retrieved by:

$$U(j\omega) = \frac{H_{rotor}(j\omega)}{Y(j\omega)}.$$

Appendix E: SISO Controller for a MIMO system

Designing SISO controllers for a MIMO system can probable done with an iterative process. In this Appendix the idea will be explained with a 2x2 MIMO process (see Figure E-1).

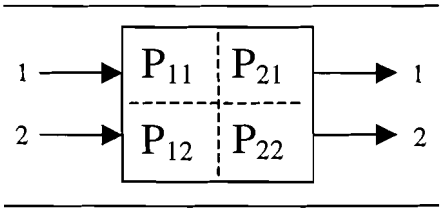

Figure E-1, 2x2 MIMO process

The iteration process will calculate in every iteration two controllers, one for the transfer from input 1 to output 1 and one for the transfer from input 2 to output 2. When the controller is calculated for one of the two transfers the other transfer is fed back with the controller calculated for this transfer during the previous iteration step.

When one of the two direct transfers is in closed loop, only one input and one output remains. For every iteration step the augmented plant of Figure 5-3 can be used, the process block will now be as given in Figure E-2 for calculating the first controller and transfer 1 will be in closed loop for calculating the second controller.

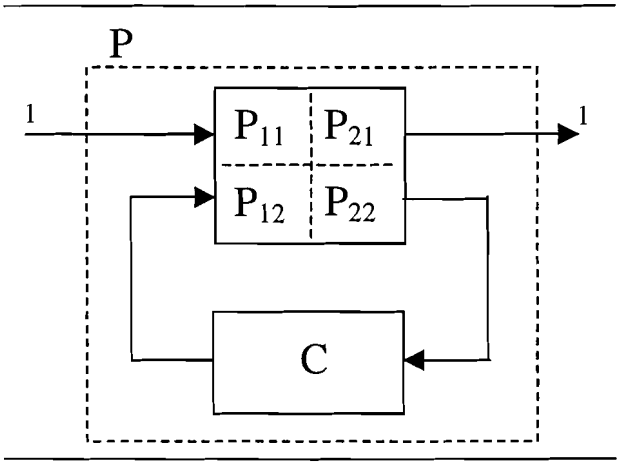

Figure E-2, process block

The iteration is done until both of the controllers are converged to their final value. The algorithm is given in Figure E-3.

The convergence of the controllers can be checked by examining the differences in bode-diagrams between the actual iteration step and the previous iteration step.

One important thing has to be mentioned. Since the order of the controller calculated is dependent of the order of the process and its weighting filters the order of the controller should be reduced after calculating a controller. Otherwise the process block will grow in order at every iteration step.

The first test results of this method were not so promising. The controller was already converged after the second iteration and was not much different from the controllers designed separately. However, it is worthwhile to do some more research into this method.

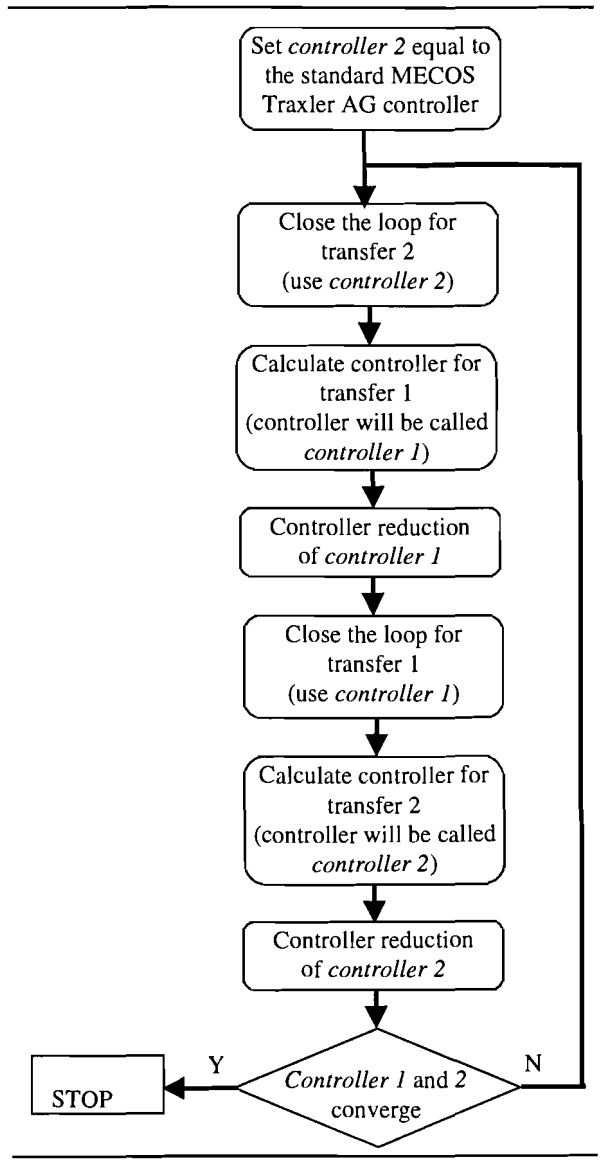

Figure E-3, algorithm for iteration

Appendix F: Recommended literature

For designing SISO controllers for a MIMO plant articles have been written. Some valuable articles are given in this Appendix. When more articles should be searched the key words *diagonal* and *decentralised* are good starting points. Also the references of the articles described in this chapter can be used.

[ABR97] Abrishamchian, M. and M.H. Kazemi

SUFFICIENT CONDITION FOR STABILITY OF DECENTRALIZED CONTROL FEEDBACK STRUCTURES

Proceedings of the 36th IEEE Conference on Decision and Control, December 10-12 1997, Hyatt Regency San Diego, San Diego, California, page 2261-2622.

The paper describes how stability can be achieved for large-scale systems by decentralised diagonal control feedback structures. The controller is obtained from the set of controllers stabilising the system consisting of the diagonal entries of the original system. An example is given in the article.

[CHA97] Chan-Gook, P., S. Duk-Sun and K. Youn-Jae

DECENTRALIZED H_∞ CONTROL WITH PERFORMANCE FOR LINEAR TIME-INVARIANT INTERCONNECTED SYSTEMS WITH TIME DELAY

Proceedings of the 36th IEEE Conference on Decision and Control, December 10-12 1997, Hyatt Regency San Diego, San Diego, California, page 2619-2620.

This paper considers the decentralised control problem of linear-time invariant interconnected systems with delays. A decentralised output-feedback controller to obtain both stability and performance of the interconnected system is designed using the standard H_∞ control theory. The article is very theoretical.

[CHI97] Chinka, D.F. and J.D. Wolfe

AN EFFICIENT DESIGN ALGORITHM FOR OPTIMAL FIXED STRUCTURE CONTROL

Proceedings of the 36th IEEE Conference on Decision and Control, December 10-12 1997, Hyatt Regency San Diego, San Diego, California, page 2625-2627.

This paper shows that an extremely flexible design method for developing optimal fixed-structure controller is to place the cost of subsystem interconnections in the cost function. The technique presented in this paper makes it possible to allow a more general class of controller gain constraints then the standard decentralised control problem. An example is given in the article.

[GRO86] Grosdidier, P. and M. Morari

INTERACTION MEASURES FOR SYSTEM UNDER DECETRALIZED CONTROL

Automatica, Vol. 22 (1986), No. 2, p. 309-319.

This paper shows that the notion of structured singular value gives a new dynamic interaction measure for multivariable systems under feedback with diagonal or block diagonal controllers. This measure can not only be used to

predict the stability of decentralised control systems but also to measure the performance loss caused by these control structures. The article is very valuable because not only a complete theoretical derivation is given but also a couple of examples.

[NET88] Nett, C.N. and J.A. Uthgenannt

AN EXPLICIT FORMULA AND AN OPTIMAL WEIGHT FOR THE 2-BLOCK STRUCTURED SINGULAR VALUE INTERACTION MEASURE

Automatica, Vol. 24 (1988), No. 2, p. 261-265.

This paper derives an explicit formula for the 2-block structured singular value interaction measure. A general, sequential algorithm for the design of stabilising decentralised controllers is developed. This algorithm makes the paper very valuable.